Title

Metabolic Control of Sensory Neuron Survival by the p75 Neurotrophin Receptor in Schwann Cells.

Journal

Journal of Neuroscience, 41(42)

ISSN

0270-6474

Authors

Follis, Rose M
Tep, Chhavy
Genaro-Mattos, Thiago C
et al.

Publication Date

2021-10-20

DOI

10.1523/jneurosci.3243-20.2021

Cellular/Molecular

Metabolic Control of Sensory Neuron Survival by the p75 Neurotrophin Receptor in Schwann Cells

Rose M. Follis,[1*] Chhavy Tep,[2*] Thiago C. Genaro-Mattos,[3] Mi Lyang Kim,[2] Jae Cheon Ryu,[2] Vivianne E. Morrison,[1] Jonah R. Chan,[4] Ned Porter,[3] Bruce D. Carter,[1#] and Sung Ok Yoon[2#]

[1]Department of Biochemistry, Vanderbilt Brain Institute, Vanderbilt University School of Medicine, Nashville, Tennessee 37232, [2]Department of Biological Chemistry and Pharmacology, Ohio State University, Columbus, Ohio, [3]Department of Chemistry, Vanderbilt University School of Arts and Sciences, Nashville, Tennessee 37232, and [4]Department of Neurology, University of California San Francisco, San Francisco, California 94158

We report that the neurotrophin receptor p75 contributes to sensory neuron survival through the regulation of cholesterol metabolism in Schwann cells. Selective deletion of p75 in mouse Schwann cells of either sex resulted in a 30% loss of dorsal root ganglia (DRG) neurons and diminished thermal sensitivity. P75 regulates Schwann cell cholesterol biosynthesis in response to BDNF, forming a co-receptor complex with ErbB2 and activating ErbB2-mediated stimulation of sterol regulatory element binding protein 2 (SREBP2), a master regulator of cholesterol synthesis. Schwann cells lacking p75 exhibited decreased activation of SREBP2 and a reduction in 7-dehydrocholesterol (7-DHC) reductase (DHCR7) expression, resulting in accumulation of the neurotoxic intermediate, 7-dehyrocholesterol in the sciatic nerve. Restoration of DHCR7 in p75 null Schwann cells in mice significantly attenuated DRG neuron loss. Together, these results reveal a mechanism by which the disruption of lipid metabolism in glial cells negatively influences sensory neuron survival, which has implications for a wide range of peripheral neuropathies.

Key words: **cholesterol; metabolism; neurotoxicity; P75; Schwann cells; sensory neurons**

Significance Statement

Although expressed in Schwann cells, the role of p75 in myelination has remained unresolved in part because of its dual expression in sensory neurons that Schwann cells myelinate. When p75 was deleted selectively among Schwann cells, myelination was minimally affected, while sensory neuron survival was reduced by 30%. The phenotype is mainly due to dysregulation of cholesterol biosynthesis in p75-deficient Schwann cells, leading to an accumulation of neurotoxic cholesterol precursor, 7-dehydrocholesterol (7-DHC). Mechanism-wise, we discovered that in response to BDNF, p75 recruits and activates ErbB2 independently of ErbB3, thereby stimulating the master regulator, sterol regulatory element binding protein 2 (SREBP2). These results together highlight a novel role of p75 in Schwann cells in regulating DRG neuron survival by orchestrating proper cholesterol metabolism.

Introduction

During peripheral nervous system development, populations of Schwann cell precursors, responding to signals from closely associated axons, undergo a highly coordinated myelination process. The ensuing formation of a lipid rich myelin sheath around medium and large caliber axons, allows for the establishment of saltatory conduction and is instrumental to the expansion and refinement of the peripheral nervous system (Woodhoo and Sommer, 2008).

It is estimated that the Schwann cell plasma membrane expands 6500-fold during myelination (Webster, 1971). Consequently, developing Schwann cells undergo an immense metabolic shift to accommodate the extraordinary magnitude of lipids and membrane proteins required for myelin generation. The majority of that expansion is fueled by the autonomous *de novo* production of lipids, which constitute 70–80% of the dry weight of myelin, 26% of which is cholesterol (Fu et al., 1998; Saher and Simons, 2010; Chrast et al., 2011). The underlying mechanisms regulating these massive alterations in lipid metabolism are, nevertheless, not well understood.

Received Dec. 31, 2020; revised Aug. 28, 2021; accepted Aug. 30, 2021.

Author contributions: S.O.Y. and B.D.C. designed research; S.O.Y., B.D.C., R.M.F., T.C.G.-M., C.T., J.C.R., V.E.M., and M.L.K. performed research; J.R.C. contributed unpublished reagents/analytic tools; S.O.Y., B.D.C., R.M.F., T.C.G.-M., N.P., C.T., and J.C.R. analyzed data; S.O.Y., B.D.C., and R.M.F. wrote the first draft of the paper; S.O.Y., B.D.C., J.R.C., and N.P. edited the paper; S.O.Y. and B.D.C. wrote the paper.

This work was supported by National Institutes of Health Grants R21 NS098362 and RO1 NS107456 (to S.O.Y. and B.D.C.).

*R.M.F. and C.T. contributed equally to this work.

#B.D.C. and S.O.Y. contributed equally to this work.

The authors declare no competing financial interests.

Correspondence should be addressed to Bruce D. Carter at bruce.carter@vanderbilt.edu or Sung Ok Yoon at sung.yoon@osumc.edu.

https://doi.org/10.1523/JNEUROSCI.3243-20.2021

There has recently been a renewed focus on Schwann cell metabolism, however, as new findings suggest that the disruption or dysregulation of lipid metabolism in Schwann cells cannot only affect myelin formation, but can also directly contribute to peripheral axon pathology; most commonly through the accumulation of neurotoxic and/or oxidative stress promoting lipid metabolites within nerves, generated by disturbed Schwann cells (Penno et al., 2010; Chrast et al., 2011; Freeman et al., 2016). The causative link between metabolic disruption in Schwann cells and resulting neuron degeneration was perhaps most dramatically demonstrated by deletion of the mitochondrial transcription factor, Tfam, in Schwann cells. Conditional Tfam knock-outs displayed marked sensory neuron degeneration in the adulthood without changes in Schwann cell viability. The degeneration phenotype was attributed to a shift in lipid metabolism in Schwann cells, which resulted in accumulation of neurotoxic acylcarnitines (Viader et al., 2013). Moreover, aberrant accumulation of Schwann cell derived neurotoxic lipids has been detected in a range of both of inherited and acquired neuropathies, including Type II diabetes, the most common cause of sensory neuropathy (Kramer et al., 2015; Atkinson et al., 2017; Gonçalves et al., 2017; Schwartzlow and Kazamel, 2019).

Here, we report that the neurotrophin receptor p75 is involved in regulating Schwann cell lipid metabolism during development. Furthermore, selective deletion of p75 in Schwann cells during embryonic development resulted in a 30% loss of dorsal root ganglia (DRG) sensory neurons, a loss we attributed to a shift in the equilibrium of cholesterol biosynthesis in Schwann cells leading to the accumulation of a highly reactive neurotoxic lipid, 7-dehydrocholesterol (7-DHC). Accordingly, restoring 7-DHC reductase (DHCR7) in Schwann cells lacking p75 was sufficient to significantly rescue sensory neuron loss. We also found that the mechanism by which p75 regulates cholesterol biosynthesis involves BDNF-mediated coupling of p75 to the tyrosine kinase receptor, ErbB2, which then induces cleavage of sterol regulatory element binding protein 2 (SREBP2), the master regulator of cholesterol synthesis (Horton et al., 2002b). Together, these results highlight a role for p75 in regulating Schwann cell lipid metabolism during development and lend support to a growing body of evidence suggesting that alterations in glia metabolism may contribute to the pathophysiology of peripheral neuropathies.

Materials and Methods

Mouse husbandry and experimental design

All experimental designs and procedures involving animals followed the guidelines of the Institutional Animal Care and Use Committee at Ohio State University and Vanderbilt University. Global p75 knock-out mice ($p75^{KO}$, RRID:IMSR_JAX:002213) have been described previously (Lee et al., 1992), and P75-floxed ($p75^{fl/fl}$) mice have been described previously (Bogenmann et al., 2011). To conditionally delete p75 from Schwann cells, $p75^{fl/fl}$ mice were first crossed with Dhh-cre (RRID: IMSR_JAX:012929; Jaegle et al., 2003). The resulting Dhh-cre+/−: $p75^{fl/-}$ mice were crossed with Dhh-cre−/−: $p75^{fl/wt}$ mice to obtain the experimental Dhh-cre+/−: $p75^{fl/fl}$ (Dhh-$p75^{\Delta}$) and the control Dhh-cre+/−: p75w/w (Dhh-$p75^{C}$) mice of either sex.

Antibodies and reagents used in the study

Antibodies actin (SC-32251), tubulin (SC-8035, RRID:AB_628408), ErbB2 (SC-284), ErbB3 (SC-285, SC-7390), and PY99 (SC-7020) were from Santa Cruz Biotechnology; V5 (R960-25), 596-Alexa Fluor goat anti-rabbit (A-11012), and 596-Alexa Fluor goat anti-mouse (catalog #A-11031 RRID:AB_141369) were from Invitrogen; and SREBP2 (catalog #557037 RRID:AB_396560) from BD Biosciences, Par3 (07–330) from Millipore, and p75 from Promega (G323A). Additional related reagents include TSA Plus Cyanine 3 (Cy3) detection kit (NEL744001KT) from PerkinElmer, Prolong antifade reagent with DAPI (P36931) from Life Technologies, and BCA Protein assay kit (23225) from Pierce.

Reagents such as 7-DHC (30800-5G-F), paraformaldehyde (P6148), chloroform (270636), fish gelatin (G7765), Triton X-100 (T8787), collagenase (C5894), collagen type 1A (C3867), Dnase I(D5025), forskolin (F6886), toluidine blue (89640), and ethyl alcohol (SHBJ7192) were from Sigma-Aldrich. Methanol (A412P), poly-D-lysine (215017525), laminin (354232), and xylene (X3F) were from Thermo Fisher Scientific. Nerve growth factor (NGF) was from Alomone (N-100), Trypsin (LS003708) from Worthington, GGF (396-HB) from R&D Systems, N2 (17502-048) and B27 (17504-044) Supplements and DMEM) 11 995–065) from Invitrogen, RNase inhibitor (N8080119) and TRIzol (15596026) from Invitrogen, DPX mounting media (13512) from EM solutions, and Hoechst 33258 (H3569) from Invitrogen. 13C-Glucose (CLM-1396-0) was obtained from Cambridge Isotope Lab. Additional reagents such as fetal bovine sera were purchased from both Hyclone (SH30088.03) and Omega Scientific (FB-01), Costar 96-well culture cluster (3595) from Costar. Both TrkB-Fc (688-TK) and control-Fc (110-HG) products were purchased from R&D Systems.

RNAscope probes were purchased from ACDbio, which included positive control probe-Mm-Ppib-C2 (313911-C2), negative control probe DapB (310043), Mm-Ntrk1-C3 (435791-C3), Mm-Ntrk2 (423611), Mm-Ntrk3-C2 (423621-C2), and Mm-Ret-C2 (431791-C2). For the actual assays, Multiplex Fluoresent Reagent kit v2 (323100) was used. TaqMan qPCR assay probes for mouse 7-dhcr (Assay number Mm00514571_m1) and Gapdh (Assay number Mm99999915_g1) were from Integrated DNA Techonologies. Taqman Fast Advanced Master Mix (4444556) was purchased from Invitrogen, while High-Capacity cDNA Reverse Transcription kit (4368814) was from Thermo Fisher Scientific. RNA was isolated using RNeay mini kit (74104) from QIAGEN.

To generate the lentivirus expressing DHCR7 gene, pLX304 vector (Addgene 25 890) was purchased to generate DHCR7-pLX304 by VectorBuilder (ccsbBroad304_06097). Lentiviruses were generated using psPax2 (12 260) and pMD2.G (12 259) from Addgene. NRG1-Type III construct was provided by Doug Falls. The sequences used to generate retrovirus constructs expressing shRNA against ErbB2 and ErbB3 in pSIREM-RetroQ-ZsGreen1were AAGTCTCACAGAGATCCTG, ACCAC GTCAAGATTACAGA, and ATCATAGTGGTATCTGTGA for ErbB2 and TCTGGACTTCCTCATCACC, GAACTTGAATGTCACATCC, and CCTGACAAGATGGAAGTAGAT for ErbB3. The sequence for the retrovirus construct expressing shRNA against p75 and Par3 were described previously (Chan et al., 2006; Vilar et al., 2009).

Thermal hyperalgesia analysis

Thermal hyperalgesia was evaluated using a modified Hargreaves Apparatus from Ugo Basile using infrared as a heat source at 50°C as we have previously published (Tep et al., 2013). Mice at the age of two to three months were subjected to the tests.

Dorsal root ganglion (DRG) morphologic analysis

L4–6 DRGs were isolated from adult [postnatal day (P)28] and juvenile (P5–P7) mice and fixed in 4% paraformaldehyde (Sigma-Aldrich catalog #P6148) or 10% neutral buffered formalin. Once imbedded in paraffin, whole DRGs were sectioned at 5 μm using a Leitz 1512 microtome. After deparaffinization and rehydration, sections were stained with toluidine blue (Sigma-Aldrich catalog #89640, 10 min), rinsed briefly in H_20, 95% ETOH, and 100% ETOH sequentially before mounted with DPX (Electron Microscopy Solutions catalog #13512). For embryonic DRG analysis, intact lumbar spine sections were processed to prevent DRG damage during isolation. DRGs were imaged in brightfield on a Nikon Eclipse Ti scope with DS-Qi2 camera (Nikon) and NIS-Elements (https://www.microscope.healthcare.nikon.com/products/software/nis-elements) at 20× magnification by a blinded individual. The first section imaged was randomly selected from sections 1–12, and

subsequently every 12th section was imaged. Images were then imported into FIJI (https://fiji.sc/) and stitched together to form whole DRG images. To determine DRG number, every neuron with a defined nuclear profile was counted using the empirical method as described in (Coggeshall et al., 1984). To determine soma diameter, each neuron included in the previous counts was outlined manually in FIJI, the area in a region of interest (ROI_ encompassing the soma) was measured, and the diameter was derived from $A = 2\pi r^2$.

Electron microscopy

Sciatic nerves were prepared for transmission electron microscopy according to Kim et al. (2003). Sciatic nerve thin sections were imaged in a randomized fashion on a Philips/FEI T-12 TEM (Phillips) electron microscope with a side mounted 2k × 2k AMT CCD camera (AMT; http://www.amtimaging.com) system at 2700× magnification. For g-ratio analysis 20 images per sample were randomly selected by a blinded evaluator and, in FIJI, images were manually thresholded to clarify myelin profiles. Then, using the ROI selection wand the area of myelinated nerve fiber cross sections and axons were calculated. The diameters of axons and myelinated fibers were derived from collected areas ($A = 2\pi r^2$) and the g-ratio (diameter of axon/diameter the myelinated fiber) was determined. To access Remak bundles, the number of distinct axons per bundle and the total number of Remak bundles per image were counted manually by a blinded observer.

RNAScope

L4–6 DRGs were isolated form P28 Dhh-p75$^{\Delta}$ and Dhh-p75^{C} mice, fixed in 4% paraformaldehyde, paraffin embedded, and sectioned at 5 μm. DRG sections with at least 150 neurons were selected from each sample for analysis, and deparaffinized as described above. As a control, sections with fewer than 50 neurons were also analyzed and were found to be consistent in distribution with the larger sections. Single-molecule fluorescence in situ hybridization was preformed using a RNAscope Multiplex Fluorescent Reagent kit v2 (ACDbio catalog #323100) and the TSA Plus Cy3 detection kit (PerkinElmer catalog #NEL744001KT) according to the manufacturer's instructions with the RNA Scopes probes described above. Fluorescent images were captured at 20× (Nikon) and analyzed in FIJI. Neurons were manually counted and ranked as being high, medium, or low expressing by a blinded observer according to a scale developed before analysis.

Retrovirus generations expressing shRNA sequences

The oligonucleotides containing the shRNA of the individual RNAi sequences were placed into pSIREN-RetroQ-ZsGreen1 vector (Clontech) using Bam HI and Xba I sites as directed by the vendor. Retroviruses were generated following transient transfection of the shRNA constructs in PlatE cells (Cell Biolabs) and the viral supernatants were concentrated by centrifugation at 20,000 rpm for 4 h at 15°C using SW28 rotor (Beckman). The viral pellet was resuspended in small volume of media and frozen at 80°C until use. For infection of Schwann cells *in vitro* and *in vivo*, a combined mixture of three different RNAi viruses were used for efficient knock-down.

Preparation of neuregulin 1 Type III

Neuregulin 1 Type III cDNA was transfected into 293T cells and the membranes were prepared according to (Taveggia et al., 2005), and the membranes were added onto Schwann cell monolayers as described (Maurel and Salzer, 2000; Taveggia et al., 2005). As a control, the membranes from untransfected 293T cells were prepared in parallel. To add the membranes to Schwann cells, 8 µg of membrane preparations was placed onto the cells and spun for 3 min at 3000 rpm.

Lipid extraction and Liquid chromatography with tandem mass spectrometry (LC-MS/MS) [selective reaction monitoring (SRM)] analysis

Sciatic nerve lipid extraction

Whole sciatic nerves were isolated and immediately frozen in liquid N_2 and stored at −80°C until the day of lipid extraction. Before extraction, nerves were ground to the consistency of a powder on dry ice with a plastic pestle to increase buffer permeability. Ice-cold NP40 lysis buffer (120 mM NaCl, 50 mM HEPES, and 1% Igepal) was added to samples and incubated for 15 min before being spun down at 15,000 rpm for 20 min. Total protein content was measured using a BCA assay (Pierce catalog #23225) and recorded for subsequent normalization. After lysis, lipids were extracted and derivatized with PTAD as described previously (Genaro-Mattos et al., 2018, 2019).

^{13}C-glucose labeling in mouse Schwann cells

Primary mouse Schwann cells were cultured as below, plated in 96 well plates, and kept in culture for 7 d before treatment. C^{13}-glucose [Cambridge Isotope Lab catalog #CLM-1396-0)-labeled DMEM media (10 mM $^{13}C_6$-glucose, 1 mM L-glutamine, 10% delipidated fetal bovine serum (FBS)] was then added and changed every 2–3 d for a total of 9 d. Live cells were then incubated with 40 ng/μl Hoechst 33258 (Invitrogen catalog #H-3569) for 20 min at 37°C and imaged under 10× magnification using ImageExpress XL (Molecular Devices) with four images collected per well. Cell number was determined by automated nuclear counting on MetaXpress 4 (https://www.moleculardevices.com/products/cellular-imaging-systems/acquisition-and-analysis-software/metaxpress#gref) for the purpose of normalization. Cells were then rinsed twice with PBS and lipids were extracted and analyzed as previously described (Genaro-Mattos et al., 2019).

Sterol analysis

Samples were placed in an Acquity UPLC system equipped with ANSI-compliant well plate holder coupled to a Thermo Scientific TSQ Quantum mass spectrometer equipped with an APCI source. Then 10 μl was injected onto the column (Phenomenex Luna Omega C18, 1.6 μm, 100 Å, 2.1 mm × 50 mm) with 100% MeOH (0.1% v/v acetic acid) mobile phase for 1.0-min runtime at a flow rate of 500 μl/min. Natural sterols were analyzed by SRM using the following transitions: Chol 369 → 369, 7-DHC 560 → 365, desmosterol 592 → 560, lanosterol 634 → 602, with retention times of 0.7, 0.4, 0.3 and 0.3 min, respectively. SRMs for the internal standards were set to: d7-Chol 376 → 376, d7-7-DHC 567 → 372, 13C3-desmosterol 595 → 563, 13C3-lanosterol 637 → 605. Final sterol numbers are reported as nmol/mg of protein.

Acylcarnitine analysis

The acylcarnitine profile was assessed by LC-MS/MS as described previously (Brittain et al., 2016). Briefly, samples were spiked with a known amount of d_3-palmitoylcarnitine as the internal standard and the lipid was extracted. After extraction, acylcarnitines were injected onto the column (Phenomenex Luna Omega C18, 1.6 μm, 100 Å, 2.1 mm × 100 mm) with 100% acetonitrile (0.1% v/v formic acid; solvent B) and water/acetonitrile (90:10 v/v, 0.1% v/v formic acid and 10 mM ammonium formate; solvent A) for 5 min runtime at a flow rate of 500 μl/min. Individual acylcarnitines were analyzed by SRM using transitions of the precursor ion (as M + H) to the respective product ions with 85 *m/z* ratio.

Primary Schwann cell culture

Rat

Primary rat Schwann cells were isolated from P2–P3 rats according to Chan et al. (2004) and maintained on collagen coated (1:20 collagen/H_20, Sigma-Aldrich catalog #C3867D) plates with high-glucose DMEM (Invitrogen catalog #11995-065) with 10% FBS (Omega catalog #FB-01) and 2 μM forskolin (Sigma-Aldrich catalog #F6886-10MG) at 37°C, 5% CO_2.

Mouse

Mouse sciatic nerves were harvested from P4–P6 C57/B6J or P75^{KO} mice and chilled in 1:1 DMEM/PBS on ice. After collection, nerves were digested at 37°C with 0.3% collagenase (Sigma-Aldrich catalog #C5894-50MG) for 15 min, after which 0.4% trypsin (Worthington catalog #LS003708) was added for subsequent 15 min; 1 ml DMEM was added to the reaction, and nerves were rinsed twice with PBS before being

manually triturated and plated to the desired density on p-D-lysine (Thermo Fisher Scientific catalog #215017525) coated plates. Cells were maintained in DMEM with 10% FBS (Hyclone catalog #SH30088.03) and 50 ng/ml GGF (R&D Systems catalog #396-HB) at 37°C, 5% CO_2.

Gene expression analysis

Primary mouse Schwann cells were lysed after 7 d in culture with 400-μl TRIzol (Invitrogen catalog #15596026) and incubated for 5 min at room temperature (RT). 100 μl Chloroform (Sigma-Aldrich catalog #270636) was added and samples were incubated for 2 min RT after mixing. The solution was spun down for 12,000 × *g* for 15 min (Sorvall-ST 16R) and the supernatant was transferred to a new tube with equal volume of 70% ETOH (Sigma-Aldrich). Total RNA was then isolated with the RNeasy Mini kit (QIAGEN catalog #74104) with QIAGEN DNase I following manufacturer's directions. To determine mRNA levels, 10 μl of the total RNA collected was reverse transcribed using the High-Capacity cDNA Reverse Transcription kit (Thermo Fischer catalog #4368814) following the manufacturer's directions. The mRNA levels of *dhcr7* and the control *Gapdh* were assessed using TaqMan (IDT) probes, assay numbers Mm00514571_m1 and Mm99999915_g1, respectively, in conjunction with Taqman Fast Advanced Master Mix (Invitrogen catalog #4444556) and the Biorad CFX96 apparatus according to the manufacturer's protocols.

Primary neuron culture

DRGs were isolated from P4–P6 rat pups and chilled in 1:1 DMEM/PBS on ice and subjected to digestion with 0.08% collagenase (Sigma-Aldrich) and 500 K.U. DNase I (Sigma-Aldrich catalog #D5025) for 30 min at 37°C, which was followed by 10 min digestion with 0.01% trypsin (Worthington). Digestion was quenched with the addition of 1 ml DMEM with 10% FBS (Hyclone) and washed in fresh DMEM before resuspension in DMEM (10% Hyclone FBS, 25 ng/ml NGF, 1% NG2, 2% B27; Invitrogen catalog #17504-044). Neurons were then plated on poly-D-lysine and laminin (Thermo Fisher Scientific)-coated plates/coverslips.

7-DHC treatment

Schwann cells

rat Schwann cells were plated at 10,000 per well in 96-well plates. The next day, they were treated 7-DHC/ETOH (Sigma-Aldrich catalog #30800-5G-F) or ETOH. The media with 7-DHC was refreshed daily, because of its oxidizable nature, until the end of the 72-h treatment period, after which the cells were stained with 40 ng/μl Hoechst (Invitrogen) for 10 min at 37°C and live imaged at 10× using the Image Express Micro XL (Molecular Devices). Four images were taken per well, which were imported into FIJI and Hoechst positive nuclei exhibiting normal morphology were counted manually by a blinded individual.

Immunofluorescence

Samples were rinsed in PBS and permeabilized for 10 min with 0.1% Triton X-100 (Sigma-Aldrich catalog #T8787). They were then blocked with 5% normal goat serum (Invitrogen catalog #16210064) for 1 h at RT and placed in primary antibody overnight. Slides were rinsed three times with PBS and incubated in secondary antibody for 1 h at RT before being rinsed three times with PBS and mounted with Prolong anti-fade reagent with DAPI (Life Technologies catalog #P36931). For paraffin embedded DRGs, 5-μm slide mounted sections were first deparaffinized and rehydrated as above, then slides were placed in a pressure cooker for 15 min (GoWise USA) within a copulin jar filled with citrate buffer antigen retrieval solution (10 mM citric acid and 0.05% Tween 20, pH 6.0). After cooling to RT, sections were permeabilized and stained in the same manner as detailed above. Antibodies used were: anti-NGFR p75 (RRID:AB_784824), anti-neurofilament (RRID:AB_91201), anti-activated caspase 3 (Cell Signaling Technology, #9661), anti-p75 ECD 9650 serum (Palmada et al., 2002), 596-Alexa Flour goat anti-mouse (RRID:AB_141369), and 647-Alexa Flour donkey anti-rabbit (RRID:AB_2536183).

Injection of lentivirus into neonate mice

Lentivirus generation

To generate lentivirus, 293T cells were transfected with Lipofectamine 2000 (Thermo Fisher Scientific catalog #11668030) with an empty pLX304 vector (Addgene #25890), or a pLX304 vector harboring a DHCR7 construct (ccsbBroad304_06097 from the CCSB-Broad Lentiviral Expression Collection) and psPax2 (Addgene #12260) and pMD2.G (Addgene #12259) constructs. At 48 h and 72 h after transfection, virus-containing media was harvested, passed through a 0.45-µm syringe filter, and combined. To concentrate the virus, the collected media was run through 100 kDa Amicon Ultra-15 Centrifugal Filter Units (Millipore-Sigma catalog #UFC910024) columns following manufacturer's directions.

Injections

Two to 3 μl of concentrated lentivirus solution was injected, using a 6 mm 31G fixed insulin needle (BD) penetrating through the outer skin, into the distal thigh of P0 neonate, Care was taken to target the intermuscular area adjoining the sciatic nerve, to avoid potential nerve damage. At P5, the sciatic nerves were harvested and stained as described in the following methods for the presence of a V5 epitope tag to confirm infection. DRGs were extracted and counting as detailed previously.

Injection of TrkB-Fc and IgG-Fc into neonate mice

TrkB-Fc and IgG-Fc were obtained from R&D Systems. Injection of Fc proteins into P0 mice sciatic nerves were performed as described (Tep et al., 2012). Briefly, 3 µl of Fc solutions (1 µg/µl) was injected using 31-G insulin syringe over the sciatic nerve midway between the knee and hip through the skin. Five days after the injection, sciatic nerves were isolated for protein extraction.

Western blotting

Western blotting was performed as described by Harrington et al. (2002).

Quantification and statistical analysis

Quantitative data are presented as mean ± SEM. All experiments were independently repeated and evaluated at least three times by a blinded individual. Prism 6/7 (GraphPad Software http://www.graphpad.com/scientific-software/prism/) was used to determine statistical significance between groups using one-way ANOVA with Tukey's *post hoc* test (for experiments with more than two groups), or Student's *t* test.

Results

Selective deletion of p75 in Schwann cells leads to minor effects on myelination

The neurotrophin receptor, p75, has long been proposed to play a role in Schwann cell myelination. P75 is highly expressed in Schwann cells both during early development and after injury, contemporaneous with many known regulators of myelination (Lemke and Chao, 1988; Jessen and Mirsky, 2016). Additionally, global p75 knock-out ($p75^{KO}$) mice exhibit a marked hypomyelination phenotype (Cosgaya et al., 2002). Deciphering the role of p75 in Schwann cell myelination has been challenging, however, mainly because of its expression in DRG sensory neurons, wherein p75 was identified as a potent regulator of neuronal survival and apoptosis. In fact, decreased trophic signaling in neurons has been primarily credited as the basis for a ~50% reduction in DRG sensory neurons and pronounced sensory deficits in $p75^{KO}$ mice (Lee et al., 1992, 1994; Murray et al., 1999).

To define the role of p75 in Schwann cells, we generated a model featuring conditional deletion of p75 in Schwann cells by crossing $p75^{fl/fl}$ mice with Desert Hedgehog-Cre transgenic mice, which express Cre recombinase in the Schwann cell lineage

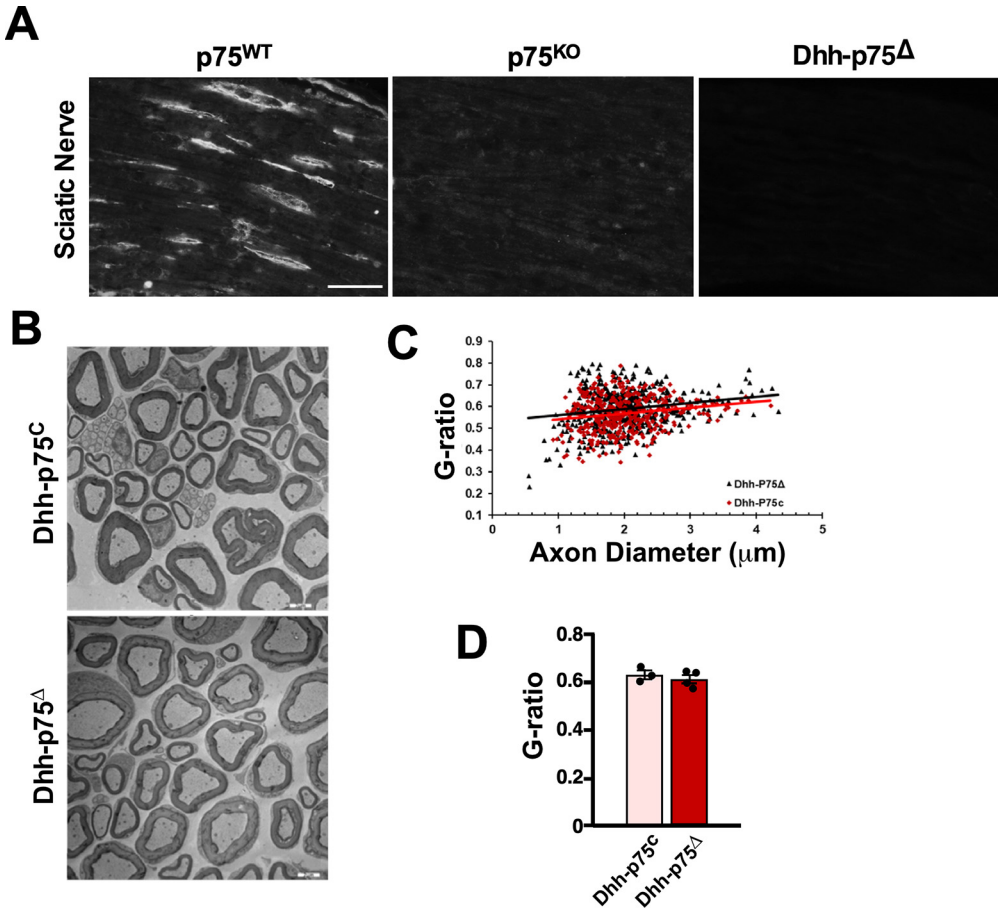

Figure 1. Deletion of p75 in Schwann cells has little effect on myelination. ***A***, Efficient deletion of p75 in Schwann cells in Dhh-p75$^{\Delta}$ mice. Adult sciatic nerves from the wild-type, p75 ^{KO}, and Dhh-p75$^{\Delta}$ mice were stained for p75. Scale bar: 25 μm. ***B***, Representative electron micrographs of P25 sciatic nerve cross sections from Dhh-P75^{C} and Dhh-p75$^{\Delta}$. Schwann cells from both genotypes exhibit grossly normal myelin and Remak morphology. Scale bar: 2 μm. ***C***, G-ratios plotted as a function of axon diameter. ***D***, Average g-ratio from P15 Dhh-p75 $^{\Delta}$ and control sciatic nerves ($N = 3$).

beginning at embryonic day (E)12 (Jaegle et al., 2003). This resulted in generation of experimental, Dhh-cre+/−: p75$^{fl/fl}$ (Dhh-p75$^{\Delta}$) and control, Dhh-cre+/−: p75w/w (Dhh-p75^{C}) mice (Fig. 1*A*). Myelin profiles of the sciatic nerve from Dhh-p75$^{\Delta}$ and Dhh-p75^{C} mice were then analyzed at P0, P5, P15 and P25 using transmission electron microscopy. To our surprise, none of the models exhibited a gross myelin deficit at any age, and only a transient and mild hypomyelination was observed in Dhh-p75$^{\Delta}$ mice at P15 compared with control (Fig. 1*B–D*). Since p75^{KO} mice show an advanced hypomyelination phenotype, these results suggest that p75 signaling in both neurons and Schwann cells must be lost to meaningfully compromise myelin formation.

Selective deletion of p75 in Schwann cells results in reduced thermal sensitivity and DRG neuron loss

P75^{KO} mice have also been noted to exhibit thermal hypoalgesia, because of a ~50% loss of sensory neurons during development. The decrease in sensory neurons was attributed to reduced survival signaling as a result of neurons lacking p75 (Lee et al., 1992; Stucky and Koltzenburg, 1997; Vaegter et al., 2011). This interpretation was also supported by a 2- to 3-fold decrease in NGF sensitivity of p75^{KO} sensory neurons, when cultured in isolation without Schwann cells (Lee et al., 1994). We, therefore, examined whether our model, absent of myelin deficits, display a thermal hypoalgesia phenotype. In agreement with previous results, P75^{KO} mice exhibited a significantly delayed response to thermal stimulation (Lee et al., 1992). Unexpectedly, however, Dhh-p75$^{\Delta}$ mice also showed significant hypoalgesia (Fig. 2*A*).

Because the thermal hypoalgesia previously noted in p75^{KO} mice was attributed primarily to their reduced sensory neuron number, we next quantified the number of DRG sensory neurons at P25–P28 in our conditional and global knock-out models. We found that Dhh-p75$^{\Delta}$ mice exhibited a surprising loss of sensory neurons, with 30% fewer DRG neurons compared with control Dhh-p75^{C} (Fig. 2*B*,*C*). In comparison, there was a 50% reduction in the number of sensory neurons in p75^{KO} mice. Given that the neuronal loss in Dhh-p75$^{\Delta}$ mice was already present at P25–P28, which is after the termination of myelination (~P14), we reasoned that the neuronal loss may occur during active Schwann cell myelination, when metabolic activity is highly up regulated to accommodate myelination. Indeed, we found a 25% decrease in the number of neurons already at P5 in Dhh-p75$^{\Delta}$ mice compared with the control (Fig. 2*D*), concurrent with large scale myelin production (Jessen et al., 2015). Taken together, these data suggest that p75 loss in developing Schwann cells significantly impacts neuronal survival in the DRG, and induces hypoalgesia.

If this is indeed the case, there should be equal number of neurons in p75^{KO} mice at E17.5, since that is well after normal developmental apoptosis is complete in DRGs (Fariñas et al., 1996; White et al., 1996), but before myelination begins. We found that there was no deficit in the number of DRG neurons

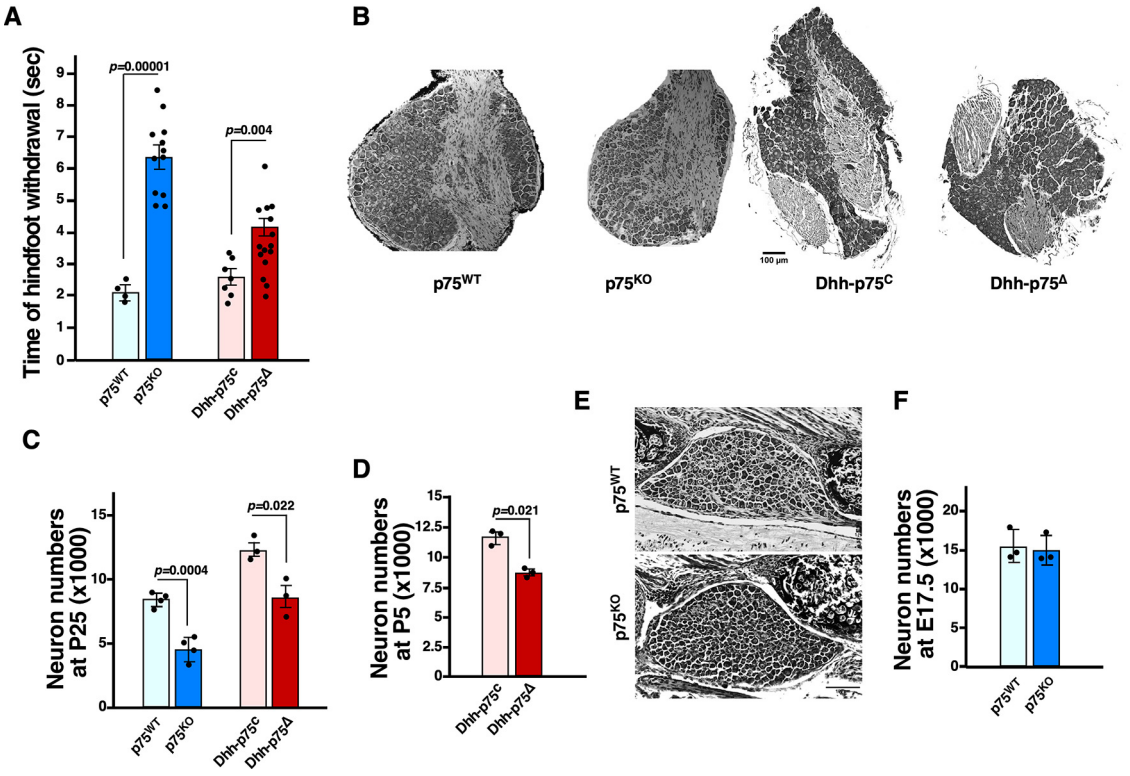

Figure 2. Deletion of p75 from Schwann cells results in a deficit of DRG sensory neurons and thermal hypoalgesia. ***A***, Mice were subjected to thermal hyperalgesia tests using a modified Hargreaves Apparatus at 50°C at two to three months of age. Student's *t* test, unpaired one-way, was used for statistics. ***B***, Representative images of DRG sections at P25–P28 from $p75^{KO}$, Dhh-$p75^{\Delta}$ and their respective controls. Scale bar: 100 μm. ***C***, Quantification of DRG neurons at P25 from $p75^{KO}$, Dhh-$p75^{\Delta}$, and their respective controls. ***D***, Quantification of DRG neurons in Dhh-$P75^{\Delta}$ and control Dhh-$P75^{C}$ mice at P5, before myelination is complete. ***E***, Representative images of DRG sections from wild type and $p75^{KO}$ at E17.5. Scale bar: 100 μm. ***F***, Quantification of DRG neurons from the wild-type and $p75^{KO}$ mice at E17.5.

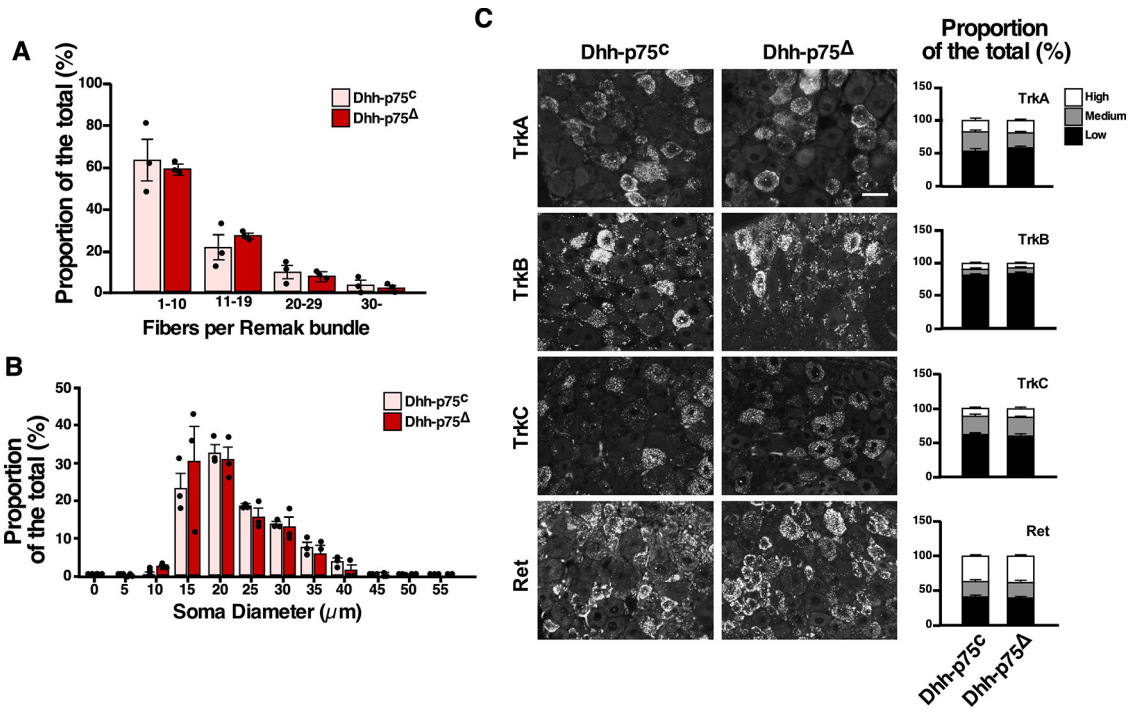

Figure 3. The loss of DRG neurons in Dhh-$p75^{\Delta}$ mice is not specific to any neuronal subtype. ***A***, Size distribution of Remak bundles in sciatic nerves of P25 Dhh-$p75^{\Delta}$ and control mice. There was no significant difference between genotypes (one-way ANOVA). ***B***, Soma size distribution of L4–6 DRGs of P25 Dhh-$p75^{\Delta}$ and control mice ($N = 3$). No significant difference was found in neuronal soma size (one-way ANOVA). ***C***, RNA scope with probes specific to TrkA, TrkB, TrkC, and Ret receptor mRNA. Representative images and quantification of L4–6 DRG sections from P25 Dhh-$p75^{\Delta}$ and control mice. Scale bar: 25 μm. Cells were evaluated as having no/low, medium, or high quantities of puncta ($N = 4$). No significant difference was found for any subtype (Student's *t* test).

Table 1. Quantification (nmol/mg protein) of cholesterol and cholesterol precursor levels in the sciatic nerves of $P75^{KO}$ and Dhh-$p75^{\Delta}$ mice compared with their respective controls, $P75^{WT}$, and Dhh-$p75^{C}$, using LC-MS/MS analysis

		Lanosterol	Desmosterol	7-DHC	8-DHC	Cholesterol
P6 sciatic nerve						
	WT ($N = 8$)	0.40 ± 0.12	0.52 ± 0.19	1.2 ± 0.16	1.3 ± 0.23	74.48 ± 17.74
	$P75^{KO}$ ($N = 5$)	0.81 ± 0.21	0.61 ± 0.20	3.9 ± 1.5	2.2 ± 0.27	72.06 ± 20.04
	p value	0.09	0.74	****$p < 0.0001$	*0.03	0.94
Adult sciatic nerve						
	WT ($N = 5$)	0.63 ± 0.046	0.74 ± 0.068	0.97 ± 0.10	1.1 ± 0.13	166.9 ± 19.04
	$P75^{KO}$ ($N = 8$)	0.62 ± 0.049	0.85 ± 0.18	1.6 ± 0.20	1.4 ± 0.19	217.7 ± 28.31
	p value	0.82	0.64	0.10	0.29	0.22
Adult sciatic nerve						
	Dhh-$P75^{C}$ ($N = 4$)	0.35 ± 0.049	0.46 ± 0.052	0.78 ± 0.064	0.80 ± 0.095	113.9 ± 10.19
	Dhh-$P75^{\Delta}$ ($N = 7$)	0.41 ± 0.014	0.59 ± 0.052	0.89 ± 0.065	0.87 ± 0.070	103 ± 5.633
	p value	0.17	0.16	0.32	0.56	0.33

Levels are displayed as mean ± SEM. One-way Student's t test was used to determine significance.

in $p75^{KO}$ mice at E17.5, despite a 50% reduction at P25–P28 (Fig. 2*E*,*F*). This result, together with our data from Dhh-$p75^{\Delta}$ mice, indicates that the absence of p75 signaling in Schwann cells is a major contributor to the loss of sensory neurons in $p75^{KO}$ mice.

The loss of DRG neurons in Dhh-$p75^{\Delta}$ mice is not specific to a particular neuronal subtype

Given the large diversity of neuronal subtypes present in DRGs, we next sought to determine whether any specific group of neurons were preferentially affected in Dhh-$p75^{\Delta}$ mice. Because p75 continues to be highly expressed in non-myelinating Remak Schwann cells throughout adulthood, and these Schwann cells enfold the unmyelinated c-fibers that respond to thermal stimuli (Murinson and Griffin, 2004), we quantified the number of axons ensheathed per Remak bundle, but found no differences (Fig. 3*A*). Additionally, there were no discernable organizational differences in Remak bundles (data not shown). As there is a general correlation between the soma size of sensory neurons and their functional subtypes (de Moraes et al., 2017), we also analyzed the distribution of soma sizes within the DRGs of Dhh-$p75^{\Delta}$ mice, but again found no significant differences (Fig. 3*B*), suggesting that there is a general reduction in all types of DRG neurons in the Dhh-$p75^{\Delta}$ mice. This conclusion was further supported when we analyzed different subtypes of DRG neurons, using RNAscope assays with subtype-specific markers, namely; TrkA for Aδ nociceptors and peptidergic nociceptors, TrkB for mechanoreceptors, TrkC for proprioceptors, or Ret for non-peptidergic nociceptors (Marmigere and Carroll, 2014). Corroborating our previous results, we found no changes in Dhh-$p75^{\Delta}$ DRGs relative to controls (Fig. 3*C*). It should be noted, these results are similar to published examinations of $p75^{KO}$ mouse DRGs, where neuron loss was found to be uniform across all sensory subtypes (Bergmann et al., 1997, 1998; Murray et al., 1999). Together, these data indicate that deletion of p75 in Schwann cells results in a global reduction in all DRG neurons, regardless of the subtype and their association with myelinating or Remak Schwann cells. We thus hypothesize the underlying mechanism of neuronal loss is likely to involve a defect in Schwann cell function capable of affecting widespread sensory neuron subtypes, rather than more localized disruption of intercellular signaling affecting only closely associated neurons.

Loss of p75 in Schwann cells results in disrupted cholesterol biosynthesis and accumulation of 7-DHC

Viader et al. (2013) demonstrated that disruption of fatty acid biosynthesis in Schwann cells led to a production of toxic acylcarnitines, which induced sensory neuron degeneration without any effect on Schwann cell viability. We thus asked whether acylcarnitine levels are similarly increased in Dhh-$p75^{\Delta}$ mice. For this analysis, lipids in the sciatic nerve from adult $p75^{KO}$, wild-type, Dhh-$p75^{\Delta}$, and Dhh-$p75^{C}$ mice were isolated and acylcarnitines were quantified by liquid chromatography-mass spectrometry (LC-MS). We, however, detected no differences in the levels of acylcarnitine species among the four genotypes (data now shown).

Previous studies have proposed that p75 plays a role in cholesterol metabolism in several cell types (Dobrowsky et al., 1994; Korade et al., 2007; Pham et al., 2016). Therefore, we analyzed cholesterol metabolites in sciatic nerves isolated from adult $p75^{KO}$, wild-type, Dhh-$p75^{\Delta}$, and Dhh-$p75^{C}$ mice. Intriguingly, although there was not a dramatic change between genotypes in the absolute levels of cholesterol or the cholesterol precursors, 7-DHC, desmosterol or lanosterol (Table 1), there was a significant increase in the ratio of 7-DHC to total cholesterol in both $p75^{KO}$ and Dhh-$p75^{\Delta}$ mice compared with respective controls (Fig. 4*A*). The accumulation of 7-DHC is noteworthy because this sterol is highly susceptible to free radical chain oxidation, producing a variety of oxysterols, including those that exert a toxic effect in Neuro2a cells and cortical neurons (Xu et al., 2009, 2012; Korade et al., 2010). Additionally, accumulation of 7-DHC is associated with the neurodegenerative disease Smith–Lemli–Opitz syndrome (SLOS; Porter and Herman, 2011).

If the increase we see in 7-DHC relative to cholesterol indicates a production of toxic lipid species sufficient to affect DRG neurons, we should then detect an increase in its ratio around the time the number of DRG neurons decrease in $p75^{KO}$ mice, that is, by P6. This is also an age when Schwann cells are actively myelinating axons and lipid biosynthesis is highly up regulated. Indeed, the ratio of 7-DHC to cholesterol was nearly 3-fold higher at P6 relative to adult in the wild-type nerve (Fig. 4*A*,*B*). Importantly, the 7-DHC to cholesterol ratio was substantially increased in the P6 $p75^{KO}$ mice compared with control, reaching 4-fold (Fig. 4*B*), a finding reflected in a significant enrichment of absolute levels of 7-DHC and 8-DHC in P6 myelinating nerves (Table 1). These results suggest that cholesterol biosynthesis is disrupted in the absence of p75 in Schwann cells, and specifically, biased toward 7-DHC accumulation over efficient conversion to cholesterol.

The analyses of cholesterol were performed using sciatic nerves, which contain axons and Schwann cells as well as various other cell types. Therefore, we repeated the same cholesterol measurements in isolated Schwann cell cultures. Mouse Schwann cells from wild-type and $p75^{KO}$ mice were

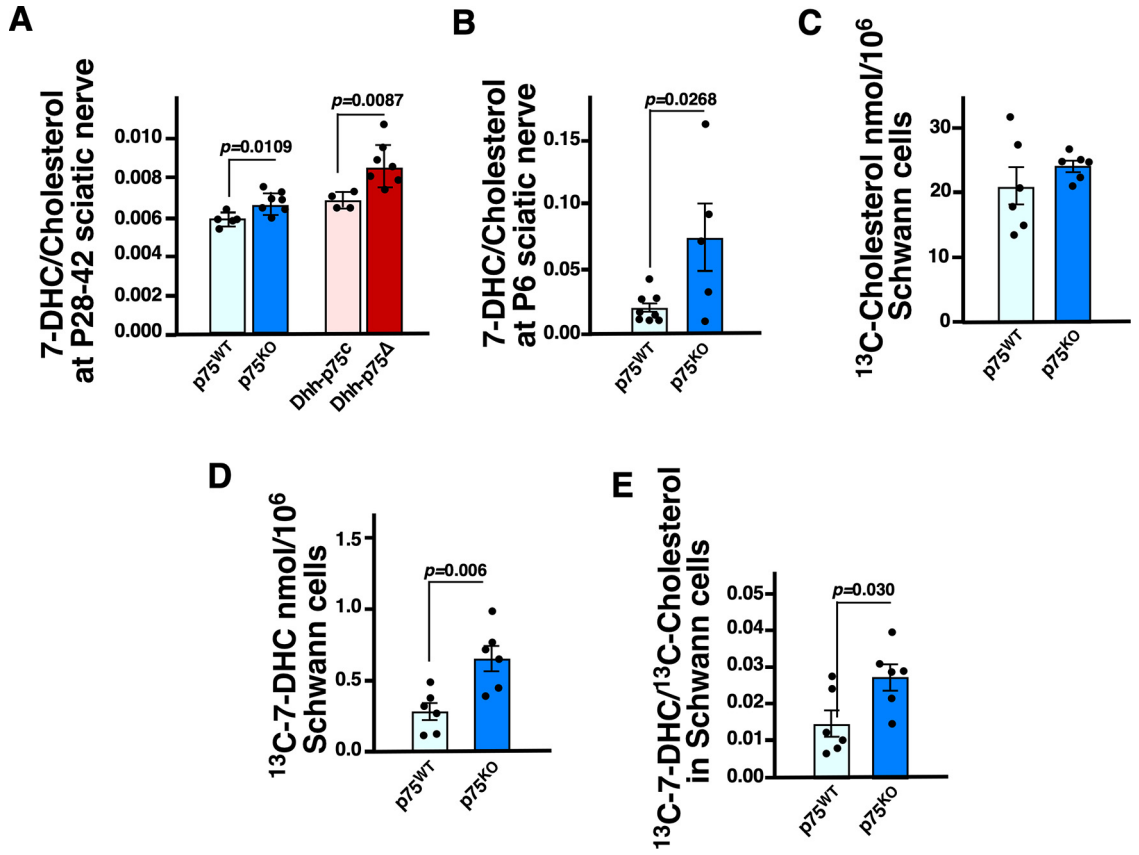

Figure 4. Deletion of p75 from Schwann cells results in elevated levels of 7-DHC, a reactive cholesterol precursor. ***A***, LC-MS/MS analysis of adult sciatic nerves from $P75^{KO}$ and Dhh-$p75^{\Delta}$ compared with their respective controls. ***B***, 7-DHC/cholesterol ratios from P6 sciatic nerve from $P75^{WT}$ and $P75^{KO}$. ***C***, ^{13}C-cholesterol generated from mouse primary Schwann cultures from $P75^{KO}$ and $P75^{WT}$ mice at P3–P6 and treated with ^{13}C-glucose in lipid depleted conditions. Lipid yield was normalized to total number cells from two independent experiments. ***D***, ^{13}C-7-DHC levels from ^{13}C-glucose-treated cells from $P75^{KO}$ mice compared with controls. ***E***, 7-DHC/cholesterol ratio from ^{13}C-glucose-treated $P75^{KO}$ and $P75^{WT}$ mouse Schwann cells.

Table 2. Levels (nmol/total cell) of C^{13}-desmosterol, C^{13}7-DHC, and C^{13}-cholesterol generated by cultured mouse primary Schwann cells harvested from $P75^{KO}$ and $P75^{WT}$ mice at P3–P6

	C13-desmosterol	C13-7-DHC	C13-cholesterol
WT ($N = 6$)	13.6 ± 0.896	0.28 ± 0.057	21.1 ± 2.95
$P75^{KO}$ ($N = 6$)	18.1 ± 2.17	0.67 ± 0.089	24.1 ± 0.856
p value	0.07	**0.006	0.34

Lipid yield was normalized to total cells in culture, $N = 6$ from two experiments. Levels are displayed as mean ± SEM. One-way Student's *t* test was used to determine significance.

cultured for 7 d in the presence of delipidated serum to maximize cholesterol production. The newly synthesized sterols were then labeled with ^{13}C-glucose supplements for nine additional days, and analyzed for sterols by LC-MS. While the amount of total ^{13}C-cholesterol was not significantly different between Schwann cells from the wild-type and $p75^{KO}$ mice (Fig. 4*C*; Table 2), the amount of ^{13}C-7-DHC was significantly higher in $p75^{KO}$ Schwann cells compared with controls (Fig. 4*D*), as well as the ratio of 7-DHC to cholesterol, which was similar to that found in the P6 nerve (Fig. 4*E*). These results suggest that the increased 7-DHC to cholesterol ratio observed in sciatic nerve samples is mostly likely because of alterations specifically in Schwann cells.

P75 regulates cholesterol biosynthesis through activation of SREBP2 in response to BDNF

During normal cholesterol biosynthesis, 7-DHC is directly, and exclusively, converted to cholesterol by DHCR7. Thus, 7-DHC accumulation occurs either from reduced DHCR7 function, as seen in SLOS pathology, or downregulation (Porter and Herman, 2011). It was previously reported that p75 knockdown resulted in a transcriptional reduction of *dhcr7* in Neuro2a cells (Korade et al., 2007). Correspondingly, we found that *dhcr7* transcript levels were significantly reduced in $p75^{KO}$ Schwann cells relative to the wild type (Fig. 5*A*). This result suggests that p75 signaling in Schwann cells is involved in transcriptional regulation of the gene encoding DHCR7, a key metabolic enzyme in cholesterol biosynthesis. The ensuing outcome is aberrant accumulation of its substrate, 7-DHC.

In considering how p75 might regulate expression of DHCR7, we considered the possible involvement of SREBP2, a master regulator of genes involved in many stages of cholesterol metabolism (Brown and Goldstein, 1997). Normally, SREBP2 is retained in the endoplasmic reticulum of cells; however, when cholesterol levels are low inside the cell, it is transported to the Golgi where it undergoes proteolytic cleavage followed by translocation to the nucleus (Horton et al., 2002a). We thus asked whether SREBP2 activation is altered in Dhh-$p75^{\Delta}$ mice compared with controls at P5. Indeed, both the levels of SREBP2 precursor and active cleaved products were significantly reduced in Dhh-$p75^{\Delta}$ nerves, compared with those of control Dhh-$p75^{C}$ mice (Fig. 5*B*,*C*). These data suggest that p75 regulates cholesterol metabolism in developing Schwann cells through modulation of SREBP2 levels and activation.

Because BDNF is released by sensory axons (Ng et al., 2007), we hypothesized that it could activate SREBP2 by binding to p75.

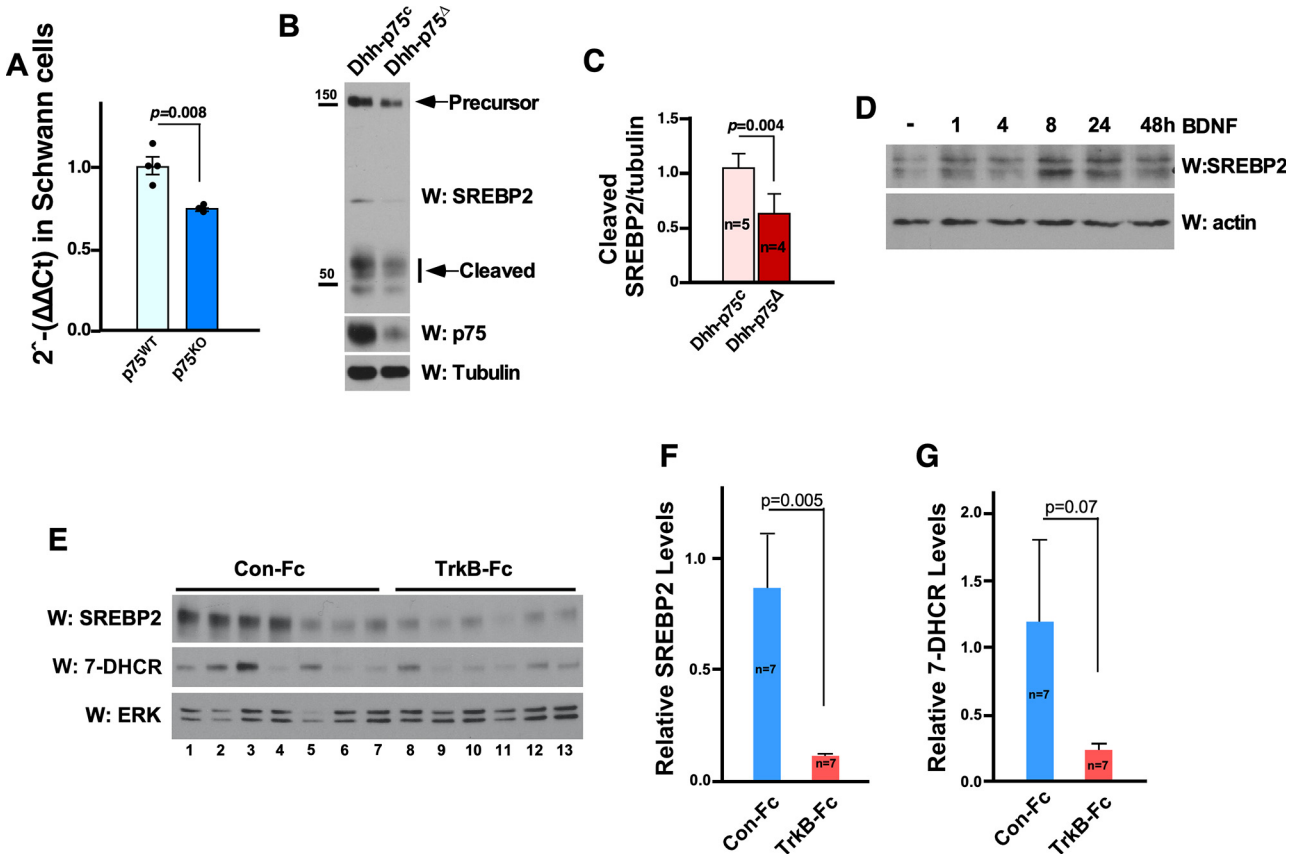

Figure 5. Loss of p75 in Schwann cells reduces dhcr7 expression and SREBP2 activation. ***A***, qPCR analysis of dhcr7 mRNA levels in primary mouse Schwann cells from $P75^{WT}$ and $P75^{KO}$ mice at P3–P6. ***B***, Representative western blot of SREBP2 precursor and active cleaved product levels from Dhh-$p75^{\Delta}$ and control sciatic nerves. ***C***, Quantification of cleaved SREBP2 over tubulin control (Student's *t* test). ***D***, BDNF stimulates SREBP2 cleavage in Schwann cells. ***E***, Squelching of BDNF action in the sciatic nerve reduced SREBP2 and 7-DHCR protein levels. Each lane represents one mouse sciatic nerve. ***F***, Quantification of SREBP2 protein levels in ***E***. ***G***, Quantification of 7-DHCR protein levels in ***E***.

Schwann cells do not express the neurotrophin receptor tyrosine kinase, TrkB (Funakoshi et al., 1993). Indeed, treatment of primary rat Schwann cells with BDNF resulted in an increase in SREBP2 cleavage products (Fig. 5*D*). To determine whether BDNF may be contributing to the SREBP2 activation *in vivo*, we injected the sciatic nerve of P0 rat pups with TrkB-Fc, which prevents it from signaling through p75 via scavenging the endogenous BDNF. There was a significant reduction in activated SREBP2 in the animals injected with TrkB-Fc, relative to control pups that were injected with IgG-Fc (Fig. 5*E*,*F*). In addition, 7-DHCR protein levels were similarly reduced with TrkB-Fc (Fig. 5*E*,*G*), although it did not reach statistical significance. These results together suggest that p75 regulates 7-DHCR levels in Schwann cells through SREBP2 in response to endogenous BDNF.

BDNF regulates SREBP2 via recruiting ErbB2 to p75 signaling pathway

We hypothesized that neuregulin signaling is one mechanism by which p75 signaling could impinge on SREBP2 and cholesterol biosynthesis, since neuregulin signaling plays a central role in virtually all areas of Schwann cell biology, including survival, migration, differentiation, and, importantly, cholesterol biosynthesis (Michailov et al., 2004; Pertusa et al., 2007; Birchmeier and Nave, 2008). In addition, p75 has been shown to suppress neuregulin signaling in Schwann cells under hyperglycemic conditions (Tan et al., 2003). Indeed, we found that while phospho-ErbB2 levels at P5–P7 sciatic nerves were significantly reduced in Dhh-$p75^{\Delta}$ mice (Fig. 6*A*,*B*), suggesting cooperative signaling between p75 and ErbB2 in Schwann cells. To test whether ErbB2 signaling is involved in the activation of SREBP2, we treated Schwann cells with BDNF in the presence of 10 μM PKI-166, an ErbB2/EGF receptor-specific inhibitor (Mellinghoff et al., 2004; Tapinos et al., 2006). PKI-166 inhibited the increase in SREBP2 cleaved products (Fig. 6*C*,*D*). Since the EGF receptor is not expressed in Schwann cells (DeClue et al., 2000), the primary target of PKI-166 is ErbB2 in these cells. These results indicate that BDNF induced SREBP2 cleavage in Schwann cells is reliant on ErbB2 activity. Indeed, BDNF addition resulted in tyrosine phosphorylation of ErbB2, albeit to a lesser extent than neuregulin (Fig. 6*E*).

ErbB2 activation by neuregulin is not through direct binding, but through forming a complex with ErbB3, which binds neuregulin (Citri et al., 2003). Surprisingly, unlike neuregulin, ErbB3 was not associated with activated ErbB2 in response to BDNF (Fig. 6*E*). We thus asked whether ErbB3 is also tyrosine phosphorylated by activated ErbB2 after BDNF treatment. While neuregulin induced robust tyrosine phosphorylation of ErbB3, BDNF failed to do so in Schwann cells (Fig. 6*F*). Similarly, knock-down of ErbB3 was effective in inhibiting tyrosine phosphorylation of ErbB2 by neuregulin, but not by BDNF (Fig. 6*G*). In contrast, knock-down of p75 prevented ErbB2 phosphorylation in response to BDNF but not neuregulin (Fig. 6*H*). Together, these results suggest that BDNF binding to p75 activates ErbB2, independent of ErbB3, leading to SREBP2 stimulation in Schwann cells.

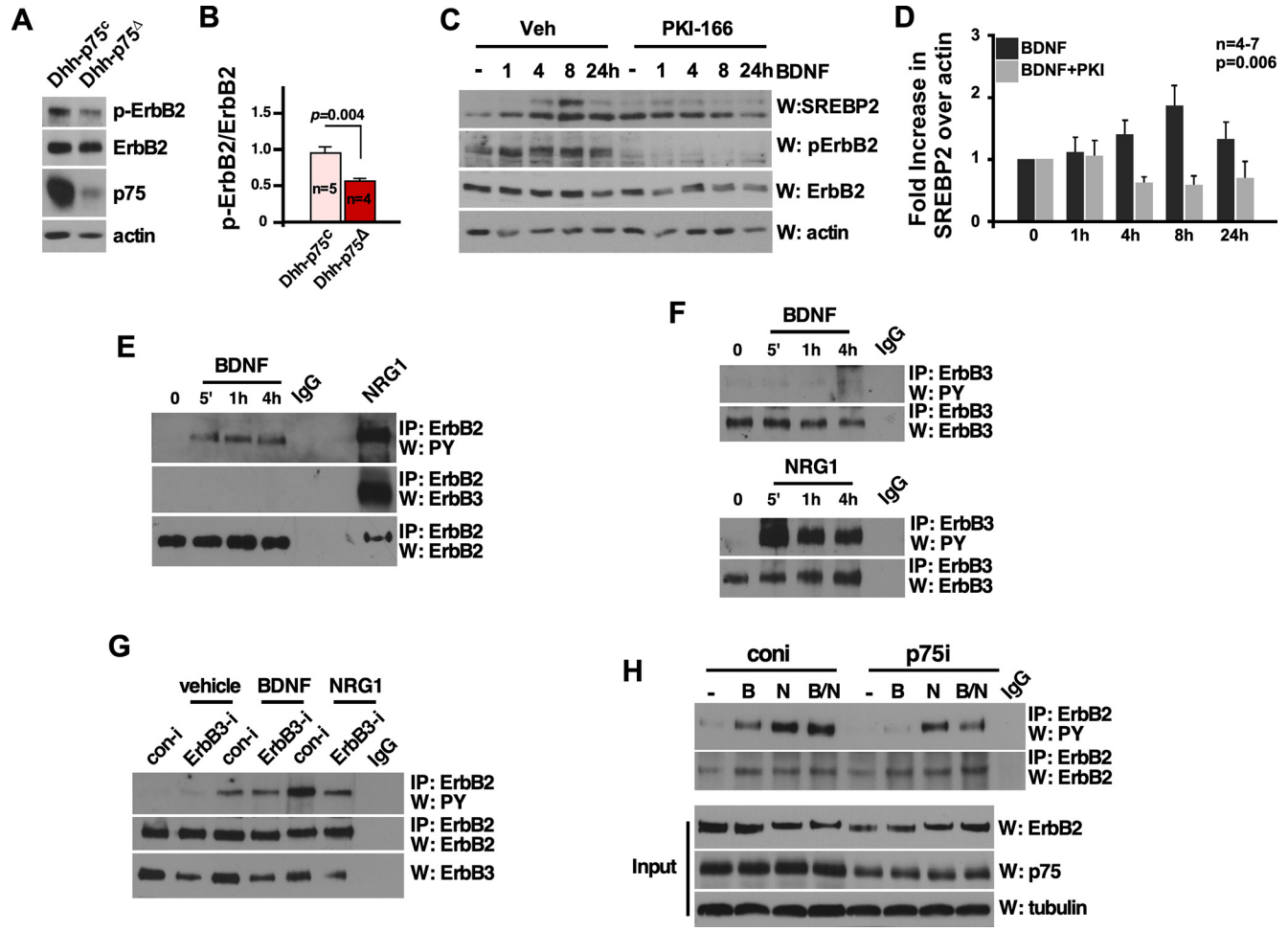

Figure 6. BDNF regulates SREBP2 via recruiting ErbB2 to p75 signaling pathway. ***A***, ErbB2 tyrosine phosphorylation in P5–P7 sciatic nerves is reduced in Dhh-p75$^{\Delta}$ compared with the control Dhh-p75^{C} mice. ***B***, Quantification of ErbB2 activation in P5–P7 sciatic nerves (Student's *t* test). ***C***, ErbB2 activity is involved in SREBP2 activation by BDNF in Schwann cells. PKI-166 at 10 μM inhibits the increase in SREBP2 cleaved products, while the vehicle (DMSO) did not. ***D***, Quantification of SREBP2 over actin controls (one-way ANOVA). ***E***, BDNF induces tyrosine phosphorylation of ErbB2 in Schwann cells. ErbB2 was immunoprecipitated and blotted with phosphotyrosine antibodies. As a positive control, the lysates from Schwann cells that had been treated with NRG1 were subjected to the same immunoprecipitation. The blot was reprobed for ErbB2 and ErbB3. ***F***, BDNF does not activate ErbB3, while neuregulin does in Schwann cells. ErbB3 was immunoprecipitated and blotted with phosphotyrosine antibodies. The blot was reprobed for ErbB3. ***G***, Knock-down of ErbB3 inhibits ErbB2 activation by NRG1, but not by BDNF. ErbB2 was immunoprecipitated and blotted with phosphotyrosine antibodies. The blot was reprobed for ErbB2. The extent of ErbB3 knock-down is shown as ErbB3 blot. ***H***, Knock-down of p75 in Schwann cells inhibits ErbB2 activation by BDNF and BDNF plus NRG1 but not by NRG1alone. The extent of p75 knock-down is shown in the p75 blot. B, BDNF; N, neuregulin.

With the surprising results that BDNF addition led to tyrosine phosphorylation of ErbB2, we asked whether p75 interacts with ErbB2. Indeed, p75 was detected in ErbB2 immunoprecipitates induced by BDNF in Schwann cells (Fig. 7*A*). Since both p75 and ErbB2 are known to interact with Par3 in Schwann cells (Chan et al., 2006; Tep et al., 2012), we asked whether the two receptors interact through Par3, a protein with three PDZ domains, capable of interacting with a large number of proteins that harbor a PDZ binding motif (Martin-Belmonte and Perez-Moreno, 2011). Par3 knock-down reduced the extent of association between ErbB2 and p75 (Fig. 7*B*). Furthermore, Par3 knock-down attenuated the extent of ErbB2 tyrosine phosphorylation without influencing neuregulin-dependent activation of ErbB2 (Fig. 7*C*).

7-DHC is toxic to DRG neurons but not to Schwann cells in culture

The accumulation of 7-DHC has been heavily implicated in the neurodegeneration associated with SLOS (Porter and Herman, 2011). Additionally, 7-DHC has been shown to be highly cytotoxic to Neuro2a cells and cortical neurons, but not astrocytes, *in vitro* (Xu et al., 2012). Therefore, we tested whether 7-DHC is cytotoxic to DRG neurons. Rat DRG neurons were treated in culture with 7-DHC and the number of live neurofilament^{+} neurons were quantified after 3 d. We found that 7-DHC was, indeed, toxic to DRG neurons, reducing the number of live neurons in a dose-dependent manner (Fig. 8). The neuronal death was because of apoptosis, based on active caspase-3 staining (Fig. 8*C*). It should be noted that DRG neurons appear to be quite sensitive to 7-DHC, which reduced the cell survival by 54% at 5 μM, a similar dose to the 1 μM that was required to reduce cell survival of cortical neurons by 60%. On the other hand, it required 50 μM of 7-DHC to reduce cell survival by 75% in Neuro2a cell lines (Korade et al., 2010; Xu et al., 2012). Unlike DRG neurons, however, rat Schwann cells were completely resistant to 7-DHC, even at the highest dose of 20 μM (Fig. 8*B*). These results support the hypothesis that aberrant accumulation of 7-DHC, while not likely to reduce Schwann cell viability, leads to sensory neuron loss.

Increasing DHCR7 levels in p75-deficient Schwann cells during early postnatal nerve development reduces sensory neurons loss

To test the hypothesis that the reduction in DHCR7 in Schwann cells is an underlying cause for the sensory neuron loss in p75-deficient mice, we sought to augment DHCR7 levels in $p75^{KO}$ early postnatal nerves and assess its effect on sensory neuron survival. We thus injected a lentivirus expressing V5-tagged DHCR7 into the mouse sciatic nerves at P0, the onset of myelination in mice (Jessen et al., 2015), and quantified the number of DRG neurons at P5. As published (Gonzalez et al., 2014), the lentivirus infected Schwann cells efficiently in the nerve based on robust V5 tag expression (Fig. 9*A*), but not DRG neurons (data not shown). When analyzed at P5, the number of DRG neurons were increased by ~35% in lenti-DHCR7 injected $p75^{KO}$ mice relative to those injected with a control lentivirus (Fig. 9*B*,*C*). A lack of complete rescue is likely because of incomplete infection of every Schwann cell. These results indicate that up-regulating DHCR7 in p75 null Schwann cells is sufficient to restore the majority of sensory neurons lost in $p75^{KO}$ mice.

Discussion

Here, we report a surprising role for p75 in Schwann cells which impacts DRG neuron survival. Deleting p75 in Schwann cells had little effect on their ability to myelinate axons but reduced sensory neuron survival by 30% and induced hypoalgesia. The loss of DRG neurons appears to be because of dysfunctional regulation of cholesterol biosynthesis in p75-deficient Schwann cells, leading to an accumulation of the highly reactive, neurotoxic cholesterol precursor, 7-DHC. In examining the mechanism by which p75 regulates cholesterol biosynthesis, we discovered that in response to BDNF, p75 recruits and activates ErbB2 independently of ErbB3, thereby stimulating the master regulator, SREBP2. These results together highlight a novel role of p75 in Schwann cells in regulating DRG neuron survival by orchestrating proper cholesterol metabolism.

As previously mentioned, there is a widely accepted and long-held supposition that developmental loss of trophic support is the underlying cause for a 50% loss of DRG neurons in $p75^{KO}$ mice. Unexpectedly, we did not observe DRG neruon loss in $p75^{KO}$ mice at E17.5, a time point well after normal developmental apoptosis is complete in DRGs (Fariñas et al., 1996; White et al., 1996). Recent studies have also presented data that conflict with the prevailing hypothesis of embryonic apoptosis. For instance, a recent report, using the neuron specific promoter, neurofilament-light chain-Cre, failed to find any changes in sensory neuron survival (Qin et al., 2020). Similarly, Chen et al. (2017) noted only a 20% reduction among the $IB4^{+}$/$peripherin^{+}$/Ret^{+} nociceptors when p75 was deleted in the DRG beginning at E12.5 in Islet1-$p75^{\Delta}$ mice. Taken together with our findings, these results indicate that reduced neurotrophic signaling, at least as it relates to normal developmental apoptosis, may not be the only cause of DRG neuron loss in p75-deficient models. Instead, our study indicates that neuronal survival is affected substantially by the loss of p75 in Schwann cells.

One signaling pathway regulated by p75 in Schwann cells identified in our study is the regulation of cholesterol biosynthesis through ErbB2-dependent activation of SREBP2 in response

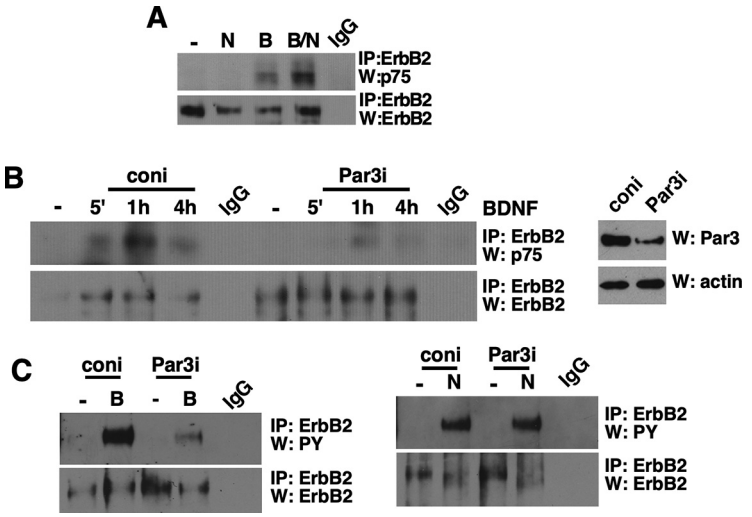

Figure 7. BDNF induces the interaction between p75 and ErbB2 receptors in Schwann cells through Par3. ***A***, p75 and ErbB2 interact in response to BDNF in Schwann cells. B, 50 ng/ml BDNF; N, 8 μg of NRG1-Type III neuregulin. ***B***, Par3 knock-down reduces the extent of interaction between p75 and ErbB2 in response to BDNF in Schwann cells. The extent of Par3 knock-down in Schwann cells is also shown. ***C***, Par3 knock-down inhibits tyrosine phosphorylation of ErbB2 by BDNF but not by NRG1-Type III.

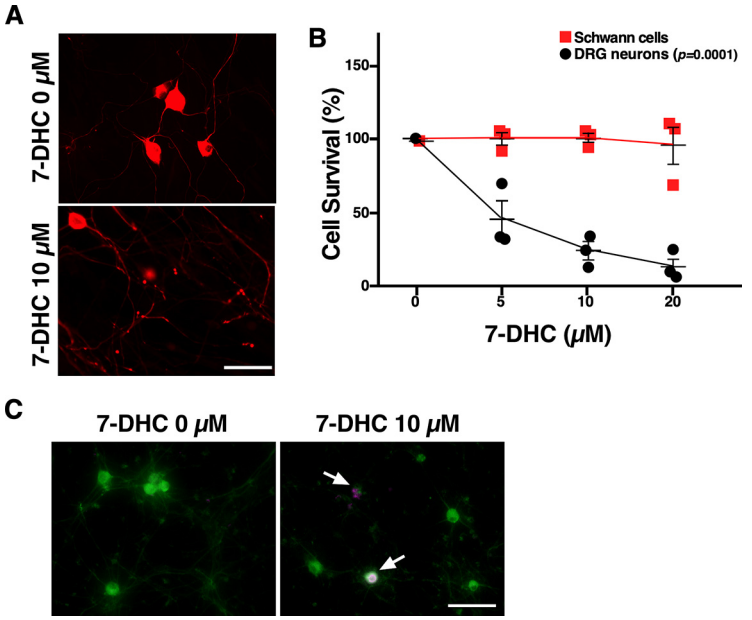

Figure 8. 7-DHC is toxic to sensory neurons but not Schwann cells. ***A***, Primary rat DRG neurons or Schwann cells were treated with varied concentrations of 7-DHC for 72 h. Representative images of DRG neuron cultures stained for neurofilament. Scale bar: 50 μm. ***B***, Quantification of DRG neurons and Schwann cells after 7-DHC treatment, $p < 0.001$, one-way ANOVA, with Tukey's *post hoc* test. ***C***, DRG neurons treated with vehicle or 7-DHC for 24 h were stained for TuJ1 and cleaved caspase 3. The arrows indicate cleaved caspase+ sensory neurons. Scale bar: 50 μm.

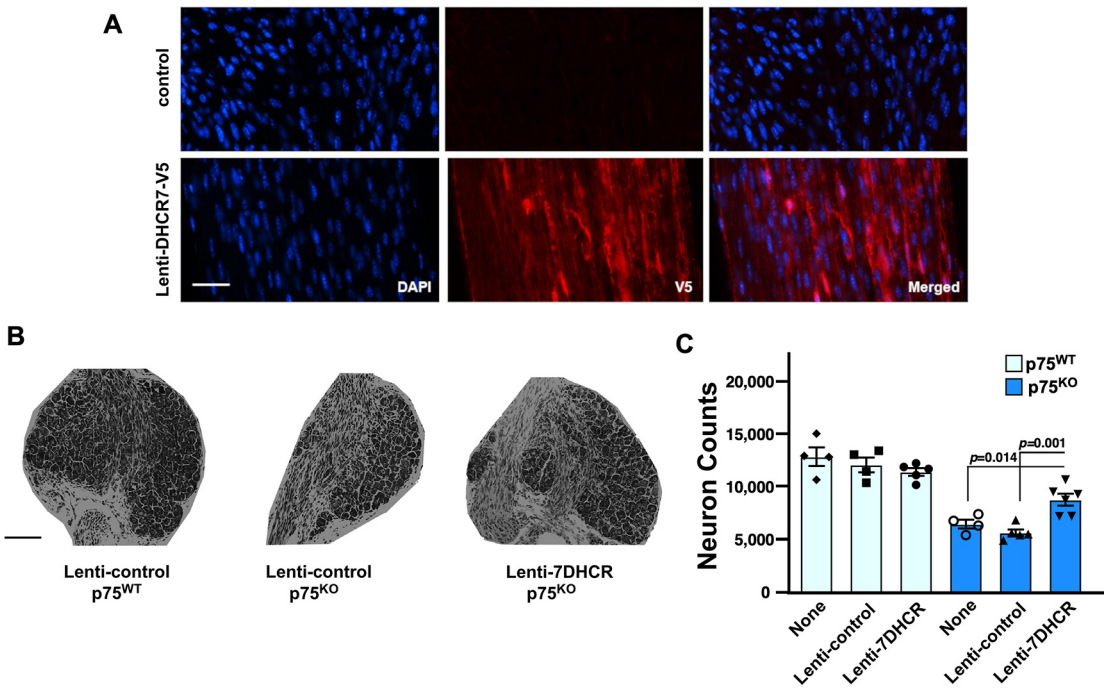

Figure 9. Increasing DHCR7 in p75-deficient Schwann cells during early postnatal nerve development rescues sensory neurons. ***A***, Staining of injected and uninjected P5 sciatic nerves for the presence of a DHCR7 fused V5 epitope tag. Scale bar: 25 μm. ***B***, Representative images of DRG sections harvested from injected and control mice. Scale bar: 100 μm. ***C***, Quantification of DRG neurons in wild-type ($p75^{WT}$) or $p75^{KO}$ mice that were uninjected (control), or injected at P0 with a lentivirus expressing DHCR7-V5 (lenti-7DHCR), or injected with a lentivirus expressing only the V5 epitope (lenti-control; $p = 0.0010$, one-way ANOVA, with Tukey's *post hoc* test; $N > 3$).

to BDNF. While a surprising finding, p75 has previously been shown to regulate SREBP2 cleavage in response to NGF in hepatocyte cell lines through the MAPK p38 (Pham et al., 2016). Whether a similar mechanism or a new signaling pathway is involved in Schwann cells is yet to be determined, but the relevant signaling pathway would have to be inhibitable by PKI-166 and Par3 knock-down. Since neuregulin is well known to regulate cholesterol metabolism through the ErbB2/ErbB3 complex, another open question is what would be the role of BDNF in stimulating cholesterol biosynthesis? We hypothesize that p75-mediated ErbB2 signaling and neuregulin-mediated ErbB2 signaling may occur in distinct locales in the developing myelin membrane, to provide exquisite spatial regulation in these highly polarized glial cells. Notably, during myelin formation, p75 becomes highly localized to the Schwann cell–axon interface through association with the polarity protein Par3 (Chan et al., 2006), placing it in a key position to respond to axonal signals.

Our findings that the cessation of p75 signaling in Schwann cells leads to both a uniform loss of DRG neurons and the accumulation of neurotoxic 7-DHC in the sciatic nerve during development is suggestive of neurodegeneration because of lipotoxicity. The exact pathomechanism of that neurodegeneration, however, requires further investigation. 7-DHC and its multiple metabolites, many of which are cell permeable oxysterols, have been theorized to cause neurodegeneration either through elevated oxidative stress, or because of adverse biological signaling activity (Tulenko et al., 2006; Korade et al., 2010; Porter and Herman, 2011; Haldar et al., 2012). Although we found elevated 7-DHC in p75 null Schwann cells contributed to the loss of DRG neurons, we cannot rule out possible involvements of other neurotoxic lipids. For example, p75 can regulate the production of ceramide, which is neurotoxic (Dobrowsky et al., 1994). An unbiased lipidomic analyses of the wild-type and $p75^{KO}$ myelinating Schwann cells would be an interesting future direction.

Regarding the mechanism by which 7-DHC could be delivered to the neurons, one possibility is through axonal incorporation of Schwann cell derived exosomes, vesicles which are largely enriched in cholesterol and have been shown to readily integrate 7-DHC (St Clair and London, 2019). Exosome transfer between Schwann cells and axons has been suggested to occur regularly during development and has been shown to profoundly impact sensory neuron health in disease models (Lopez-Verrilli and Court, 2012; Zhou et al., 2018; Wang et al., 2020). A mechanism of direct transfer, which is not reliant on passive neuronal lipid uptake, as our 7-DHC *in vitro* experiments were, could also greatly affect localized 7-DHC concentrations. Given that sensory axons are completely ensheathed by Schwann cells, either via myelin or Remak bundling, the close proximity between these cells likely results in relatively high local concentrations of 7-DHC, which could amplify any neurotoxic effects, particularly during sensitive developmental windows.

The unique lipid signaling between Schwann cells and neurons described here corroborates a growing body of literature indicating that Schwann cell metabolism has a profound effect on neuron function and survival (Jha and Morrison, 2018). Schwann cells are essential for the survival of sensory neurons (Davies, 1998; Woldeyesus et al., 1999; Chen et al., 2003); however, exactly how they regulate neuron viability and activity is poorly understood. In pathologic conditions, such as diabetes (Feldman et al., 2017; Gonçalves et al., 2017) and some forms of Charcot–Marie–Tooth (CMT) disease (Brennan et al., 2015), disruption of Schwann cell metabolism has been suggested to contribute to neurodegeneration through maladaptive changes in mitochondria after hyperglycemia induced oxidative stress (Figueroa-Romero et al., 2008; Askwith et al., 2009; Zhang et al., 2010; Cinci et al., 2015). Such dysfunctional mitochondria in Schwann cells may result in the production of neurotoxic lipids capable of inducing neurodegeneration without obvious effects

on Schwann cell viability (Viader et al., 2011, 2013). Why Schwann cells are more resistant to some toxic lipid species is not clear. However, it is notable that these cells are programmed to produce enormous quantities of lipids, including cholesterol, to form myelin (Saher and Simons, 2010). Thus, it is reasonable to expect that mechanisms to cope with toxic metabolites evolved in these cells.

Alterations in Schwann cell metabolism and neurotoxic lipid accumulation, has been found to be a primary pathomechanism in several inherited neuropathies including hereditary sensory and autonomic neuropathy 1 (HSN1), a rare form of axonal CMT2 (AR-CMT2), and several sphingomyelinases with peripheral nerve symptomology such as Krabbe disease (Penno et al., 2010; Spassieva and Bieberich, 2016; Atkinson et al., 2017; Schwartzlow and Kazamel, 2019). Together with our results, these findings indicate that exploring mechanisms of Schwann cell metabolic dysfunction in inherited neuropathies may inform our understanding of the complex pathophysiology of more common acquired neuropathies.

References

Askwith T, Zeng W, Eggo MC, Stevens MJ (2009) Oxidative stress and dysregulation of the taurine transporter in high-glucose-exposed human Schwann cells: implications for pathogenesis of diabetic neuropathy. Am J Physiol Endocrinol Metab 297:E620–E628.

Atkinson D, Nikodinovic Glumac J, Asselbergh B, Ermanoska B, Blocquel D, Steiner R, Estrada-Cuzcano A, Peeters K, Ooms T, De Vriendt E, Yang XL, Hornemann T, Milic Rasic V, Jordanova A (2017) Sphingosine 1-phosphate lyase deficiency causes Charcot-Marie-Tooth neuropathy. Neurology 88:533–542.

Bergmann I, Priestley JV, McMahon SB, Bröcker EB, Toyka KV, Koltzenburg M (1997) Analysis of cutaneous sensory neurons in transgenic mice lacking the low affinity neurotrophin receptor p75. Eur J Neurosci 9:18–28.

Bergmann I, Reiter R, Toyka KV, Koltzenburg M (1998) Nerve growth factor evokes hyperalgesia in mice lacking the low-affinity neurotrophin receptor p75. Neurosci Lett 255:87–90.

Birchmeier C, Nave K-A (2008) Neuregulin-1, a key axonal signal that drives Schwann cell growth and differentiation. Glia 56:1491–1497.

Bogenmann E, Thomas PS, Li Q, Kim J, Yang L-T, Pierchala B, Kaartinen V (2011) Generation of mice with a conditional allele for the p75(NTR) neurotrophin receptor gene. Genesis 49:862–869.

Brennan KM, Bai Y, Shy ME (2015) Demyelinating CMT–what's known, what's new and what's in store? Neurosci Lett 596:14–26.

Brittain EL, Talati M, Fessel JP, Zhu H, Penner N, Calcutt MW, West JD, Funke M, Lewis GD, Gerszten RE, Hamid R, Pugh ME, Austin ED, Newman JH, Hemnes AR (2016) Fatty acid metabolic defects and right ventricular lipotoxicity in human pulmonary arterial hypertension. Circulation 133:1936–1944.

Brown MS, Goldstein JL (1997) The SREBP pathway: regulation of cholesterol metabolism by proteolysis of a membrane-bound transcription factor. Cell 89:331–340.

Chan JR, Jolicoeur C, Yamauchi J, Elliott J, Fawcett JP, Ng BK, Cayouette M (2006) The polarity protein Par-3 directly interacts with p75NTR to regulate myelination. Science 314:832–836.

Chan JR, Watkins TA, Cosgaya JM, Zhang C, Chen L, Reichardt LF, Shooter EM, Barres BA (2004) NGF controls axonal receptivity to myelination by Schwann cells or oligodendrocytes. Neuron 43:183–191.

Chen S, Rio C, Ji RR, Dikkes P, Coggeshall RE, Woolf CJ, Corfas G (2003) Disruption of ErbB receptor signaling in adult non-myelinating Schwann cells causes progressive sensory loss. Nat Neurosci 6:1186–1193.

Chen Z, Donnelly CR, Dominguez B, Harada Y, Lin W, Halim AS, Bengoechea TG, Pierchala BA, Lee KF (2017) p75 is required for the establishment of postnatal sensory neuron diversity by potentiating Ret signaling. Cell Rep 21:707–720.

Chrast R, Saher G, Nave K-A, Verheijen MHG (2011) Lipid metabolism in myelinating glial cells: lessons from human inherited disorders and mouse models. J Lipid Res 52:419–434.

Cinci L, Corti F, Di Cesare Mannelli L, Micheli L, Zanardelli M, Ghelardini C (2015) Oxidative, metabolic, and apoptotic responses of Schwann cells to high glucose levels. J Biochem Mol Toxicol 29:274–279.

Citri A, Skaria KB, Yarden Y (2003) The deaf and the dumb: the biology of ErbB-2 and ErbB-3. Exp Cell Res 284:54–65.

Coggeshall RE, Chung K, Greenwood D, Hulsebosch CE (1984) An empirical method for converting nucleolar counts to neuronal numbers. J Neurosci Methods 12:125–132.

Cosgaya JM, Chan JR, Shooter EM (2002) The neurotrophin receptor p75NTR as a positive modulator of myelination. Science 298:1245–1248.

Davies AM (1998) Neuronal survival: early dependence on Schwann cells. Curr Biol 8:R15–R18.

de Moraes ER, Kushmerick C, Naves LA (2017) Morphological and functional diversity of first-order somatosensory neurons. Biophys Rev 9:847–856.

DeClue JE, Heffelfinger S, Benvenuto G, Ling B, Li S, Rui W, Vass WC, Viskochil D, Ratner N (2000) Epidermal growth factor receptor expression in neurofibromatosis type 1-related tumors and NF1 animal models. J Clin Invest 105:1233–1241.

Dobrowsky RT, Werner MH, Castellino AM, Chao MV, Hannun YA (1994) Activation of the sphingomyelin cycle through the low-affinity neurotrophin receptor. Science 265:1596–1599.

Fariñas I, Yoshida CK, Backus C, Reichardt LF (1996) Lack of neurotrophin-3 results in death of spinal sensory neurons and premature differentiation of their precursors. Neuron 17:1065–1078.

Feldman EL, Nave KA, Jensen TS, Bennett DLH (2017) New horizons in diabetic neuropathy: mechanisms, bioenergetics, and pain. Neuron 93:1296–1313.

Figueroa-Romero C, Sadidi M, Feldman EL (2008) Mechanisms of disease: the oxidative stress theory of diabetic neuropathy. Rev Endocr Metab Disord 9:301–314.

Freeman OJ, Unwin RD, Dowsey AW, Begley P, Ali S, Hollywood KA, Rustogi N, Petersen RS, Dunn WB, Cooper GJS, Gardiner NJ (2016) Metabolic dysfunction is restricted to the sciatic nerve in experimental diabetic neuropathy. Diabetes 65:228–238.

Fu Q, Goodrum JF, Hayes C, Hostettler JD, Toews AD, Morell P (1998) Control of cholesterol biosynthesis in Schwann cells. J Neurochem 71:549–555.

Funakoshi H, Frisén J, Barbany G, Timmusk T, Zachrisson O, Verge VM, Persson H (1993) Differential expression of mRNAs for neurotrophins and their receptors after axotomy of the sciatic nerve. J Cell Biol 123:455–465.

Genaro-Mattos TC, Tallman KA, Allen LB, Anderson A, Mirnics K, Korade Z, Porter NA (2018) Dichlorophenyl piperazines, including a recently-approved atypical antipsychotic, are potent inhibitors of DHCR7, the last enzyme in cholesterol biosynthesis. Toxicol Appl Pharmacol 349:21–28.

Genaro-Mattos TC, Allen LB, Anderson A, Tallman KA, Porter NA, Korade Z, Mirnics K (2019) Maternal aripiprazole exposure interacts with 7-dehydrocholesterol reductase mutations and alters embryonic neurodevelopment. Mol Psychiatry 24:491–500.

Gonçalves NP, Vægter CB, Andersen H, Østergaard L, Calcutt NA, Jensen TS (2017) Schwann cell interactions with axons and microvessels in diabetic neuropathy. Nat Rev Neurol 13:135–147.

Gonzalez S, Fernando RN, Perrin-tricaud C, Tricaud N (2014) In vivo introduction of transgenes into mouse sciatic nerve cells in situ using viral vectors. Nat Protoc 9:1160–1169.

Haldar S, Kanaparthi RK, Samanta A, Chattopadhyay A (2012) Differential effect of cholesterol and its biosynthetic precursors on membrane dipole potential. Biophys J 102:1561–1569.

Harrington AW, Kim JY, Yoon SO (2002) Activation of Rac GTPase by p75 is necessary for c-jun N-terminal kinase-mediated apoptosis. J Neurosci 22:156–166.

Horton JD, Goldstein JL, Brown MS (2002a) SREBPs: activators of the complete program of cholesterol and fatty acid synthesis in the liver. J Clin Invest 109:1125–1131.

Horton JD, Goldstein JL, Brown MS (2002b) SREBPs: transcriptional mediators of lipid homeostasis. Cold Spring Harb Symp Quant Biol 67:491–498.

Jaegle M, Ghazvini M, Mandemakers W, Piirsoo M, Driegen S, Levavasseur F, Raghoenath S, Grosveld F, Meijer D (2003) The POU proteins Brn-2 and Oct-6 share important functions in Schwann cell development. Genes Dev 17:1380–1391.

Jessen K, Mirsky R (2016) The repair Schwann cell and its function in regenerating nerves. J Physiol 594:3521–3531.

Jessen KR, Mirsky R, Lloyd AC (2015) Schwann cells: development and role in nerve repair. Cold Spring Harb Perspect Biol 7:a020487.

Jha MK, Morrison BM (2018) Glia-neuron energy metabolism in health and diseases: new insights into the role of nervous system metabolic transporters. Exp Neurol 309:23–31.

Kim JY, Sun Q, Oglesbee M, Yoon SO (2003) The role of ErbB2 signaling in the onset of terminal differentiation of oligodendrocytes in vivo. J Neurosci 23:5561–5571.

Korade Z, Mi Z, Portugal C, Schor NF (2007) Expression and p75 neurotrophin receptor dependence of cholesterol synthetic enzymes in adult mouse brain. Neurobiol Aging 28:1522–1531.

Korade Z, Xu L, Shelton R, Porter NA (2010) Biological activities of 7-dehydrocholesterol-derived oxysterols: implications for Smith-Lemli-Opitz syndrome. J Lipid Res 51:3259–3269.

Kramer R, Bielawski J, Kistner-Griffin E, Othman A, Alecu I, Ernst D, Kornhauser D, Hornemann T, Spassieva S (2015) Neurotoxic 1-deoxysphingolipids and paclitaxel-induced peripheral neuropathy. FASEB J 29:4461–4472.

Lee KF, Li E, Huber LJ, Landis SC, Sharpe AH, Chao MV, Jaenisch R (1992) Targeted mutation of the gene encoding the low affinity NGF receptor p75 leads to deficits in the peripheral sensory nervous system. Cell 69:737–749.

Lee KF, Davies AM, Jaenisch R (1994) p75-deficient embryonic dorsal root sensory and neonatal sympathetic neurons display a decreased sensitivity to NGF. Development 120:1027–1033.

Lemke G, Chao M (1988) Axons regulate Schwann cell expression of the major myelin and NGF receptor genes. Development 102:499–504.

Lopez-Verrilli MA, Court FA (2012) Transfer of vesicles from Schwann cells to axons: a novel mechanism of communication in the peripheral nervous system. Front Physiol 3:205.

Marmigere F, Carroll P (2014) Neurotrophin signalling and transcription programmes interactions in the development of somatosensory neurons. Handb Exp Pharmacol 220:329–353.

Martin-Belmonte F, Perez-Moreno M (2011) Epithelial cell polarity, stem cells and cancer. Nat Rev Cancer 12:23–38.

Maurel P, Salzer JL (2000) Axonal regulation of Schwann cell proliferation and survival and the initial events of myelination requires PI 3-kinase activity. J Neurosci 20:4635–4645.

Mellinghoff IK, Vivanco I, Kwon A, Tran C, Wongvipat J, Sawyers CL (2004) HER2/neu kinase-dependent modulation of androgen receptor function through effects on DNA binding and stability. Cancer Cell 6:517–527.

Michailov GV, Sereda MW, Brinkmann BG, Fischer TM, Haug B, Birchmeier C, Role L, Lai C, Schwab MH, Nave KA (2004) Axonal neuregulin-1 regulates myelin sheath thickness. Science 304:700–703.

Murinson BB, Griffin JW (2004) C-fiber structure varies with location in peripheral nerve. J Neuropathol Exp Neurol 63:246–254.

Murray SS, Bartlett PF, Cheema SS (1999) Differential loss of spinal sensory but not motor neurons in the p75NTR knockout mouse. Neurosci Lett 267:45–48.

Ng BK, Chen L, Mandemakers W, Cosgaya JM, Chan JR (2007) Anterograde transport and secretion of brain-derived neurotrophic factor along sensory axons promote Schwann cell myelination. J Neurosci 27:7597–7603.

Palmada M, Kanwal S, Rutkoski NJ, Gustafson-Brown C, Johnson RS, Wisdom R, Carter BD, Gufstafson-Brown C (2002) c-jun is essential for sympathetic neuronal death induced by NGF withdrawal but not by p75 activation. J Cell Biol 158:453–461.

Penno A, Reilly MM, Houlden H, Laurá M, Rentsch K, Niederkofler V, Stoeckli ET, Nicholson G, Eichler F, Brown RH, von Eckardstein A, Hornemann T (2010) Hereditary sensory neuropathy type 1 is caused by the accumulation of two neurotoxic sphingolipids. J Biol Chem 285:11178–11187.

Pertusa M, Morenilla-Palao C, Carteron C, Viana F, Cabedo H (2007) Transcriptional control of cholesterol biosynthesis in Schwann cells by axonal neuregulin 1. J Biol Chem 282:28768–28778.

Pham DD, Do HT, Bruelle C, Kukkonen JP, Eriksson O, Mogollón I, Korhonen LT, Arumäe U, Lindholm D (2016) p75 neurotrophin receptor signaling activates sterol regulatory element-binding protein-2 in hepatocyte cells via p38 mitogen-activated protein kinase and caspase-3. J Biol Chem 291:10747–10758.

Porter FD, Herman GE (2011) Malformation syndromes caused by disorders of cholesterol synthesis. J Lipid Res 52:6–34.

Qin Z, Gonsalvez DG, Wood RJ, Daemi F, Yoo S, Ivanusic JJ, Coulson EJ, Murray SS, Xiao J (2020) Partial deletion of p75(NTR) in large-diameter DRG neurons exerts no influence upon the survival of peripheral sensory neurons in vivo. J Neurosci Res 98:1987–1998.

Saher G, Simons M (2010) Cholesterol and myelin biogenesis, pp 489–508. Dordrecht: Springer.

Schwartzlow C, Kazamel M (2019) Hereditary sensory and autonomic neuropathies: adding more to the classification. Curr Neurol Neurosci Rep 19:52.

Spassieva S, Bieberich E (2016) Lysosphingolipids and sphingolipidoses: psychosine in Krabbe's disease. J Neurosci Res 94:974–981.

St Clair JW, London E (2019) Effect of sterol structure on ordered membrane domain (raft) stability in symmetric and asymmetric vesicles. Biochim Biophys Acta Biomembr 1861:1112–1122.

Stucky CL, Koltzenburg M (1997) The low-affinity neurotrophin receptor p75 regulates the function but not the selective survival of specific subpopulations of sensory neurons. J Neurosci 17:4398–4405.

Tan W, Rouen S, Barkus KM, Dremina YS, Hui D, Christianson JA, Wright DE, Yoon SO, Dobrowsky RT (2003) Nerve growth factor blocks the glucose-induced down-regulation of caveolin-1 expression in Schwann cells via p75 neurotrophin receptor signaling. J Biol Chem 278:23151–23162.

Tapinos N, Ohnishi M, Rambukkana A (2006) ErbB2 receptor tyrosine kinase signaling mediates early demyelination induced by leprosy bacilli. Nat Med 12:961–966.

Taveggia C, Zanazzi G, Petrylak A, Yano H, Rosenbluth J, Einheber S, Xu X, Esper RM, Loeb JA, Shrager P, Chao MV, Falls DL, Role L, Salzer JL (2005) Neuregulin-1 type III determines the ensheathment fate of axons. Neuron 47:681–694.

Tep C, Kim ML, Opincariu LI, Limpert AS, Chan JR, Appel B, Carter BD, Yoon SO (2012) Brain-derived neurotrophic factor (BDNF) induces polarized signaling of small GTPase (Rac1) protein at the onset of Schwann cell myelination through partitioning-defective 3 (Par3) protein. J Biol Chem 287:1600–1608.

Tep C, Lim TH, Ko PO, Getahun S, Ryu JC, Goettl VM, Massa SM, Basso M, Longo FM, Yoon SO (2013) Oral administration of a small molecule targeted to block proNGF binding to p75 promotes myelin sparing and functional recovery after spinal cord injury. J Neurosci 33:397–410.

Tulenko TN, Boeze-Battaglia K, Mason RP, Tint GS, Steiner RD, Connor WE, Labelle EF (2006) A membrane defect in the pathogenesis of the Smith-Lemli-Opitz syndrome. J Lipid Res 47:134–143.

Vaegter CB, Jansen P, Fjorback AW, Glerup S, Skeldal S, Kjolby M, Richner M, Erdmann B, Nyengaard JR, Tessarollo L, Lewin GR, Willnow TE, Chao MV, Nykjaer A (2011) Sortilin associates with Trk receptors to enhance anterograde transport and neurotrophin signaling. Nat Neurosci 14:54–61.

Viader A, Golden JP, Baloh RH, Schmidt RE, Hunter DA, Milbrandt J (2011) Schwann cell mitochondrial metabolism supports long-term axonal survival and peripheral nerve function. J Neurosci 31:10128–10140.

Viader A, Sasaki Y, Kim S, Strickland A, Workman CS, Yang K, Gross RW, Milbrandt J (2013) Aberrant Schwann cell lipid metabolism linked to mitochondrial deficits leads to axon degeneration and neuropathy. Neuron 77:886–898.

Vilar M, Charalampopoulos I, Kenchappa RS, Simi A, Karaca E, Reversi A, Choi S, Bothwell M, Mingarro I, Friedman WJ, Schiavo G, Bastiaens PI, Verveer PJ, Carter BD, Ibáñez CF (2009) Activation of the p75 neurotrophin receptor through conformational rearrangement of disulphide-linked receptor dimers. Neuron 62:72–83.

Wang L, Chopp M, Szalad A, Lu X, Zhang Y, Wang X, Cepparulo P, Lu M, Li C, Zhang ZG (2020) Exosomes derived from Schwann cells ameliorate peripheral neuropathy in type 2 diabetic mice. Diabetes 69:749–759.

Webster HD (1971) The geometry of peripheral myelin sheaths during their formation and growth in rat sciatic nerves. J Cell Biol 48:348–367.

White FA, Silos-Santiago I, Molliver DC, Nishimura M, Phillips H, Barbacid M, Snider WD (1996) Synchronous onset of NGF and TrkA survival dependence in developing dorsal root ganglia. J Neurosci 16:4662–4672.

Woldeyesus MT, Britsch S, Riethmacher D, Xu L, Sonnenberg-Riethmacher E, Abou-Rebyeh F, Harvey R, Caroni P, Birchmeier C (1999) Peripheral nervous system defects in erbB2 mutants following genetic rescue of heart development. Genes Dev 13:2538–2548.

Woodhoo A, Sommer L (2008) Development of the Schwann cell lineage: from the neural crest to the myelinated nerve. Glia 56:1481–1490.

Xu G, Guan L, Sun J, Chen ZY (2009) Oxidation of cholesterol and beta-sitosterol and prevention by natural antioxidants. J Agric Food Chem 57:9284–9292.

Xu L, Mirnics K, Bowman AB, Liu W, Da J, Porter NA, Korade Z (2012) DHCEO accumulation is a critical mediator of pathophysiology in a Smith-Lemli-Opitz syndrome model. Neurobiol Dis 45:923–929.

Zhang L, Yu C, Vasquez FE, Galeva N, Onyango I, Swerdlow RH, Dobrowsky RT (2010) Hyperglycemia alters the Schwann cell mitochondrial proteome and decreases coupled respiration in the absence of superoxide production. J Proteome Res 9:458–471.

Zhou M, Hu M, He S, Li B, Liu C, Min J, Hong L (2018) Effects of RSC96 Schwann cell-derived exosomes on proliferation, senescence, and apoptosis of dorsal root ganglion cells in v. Med Sci Monit 24:7841–7849.